JACS
JOURNAL OF THE AMERICAN CHEMICAL SOCIETY

ARTICLE

pubs.acs.org/JACS

Electronic Structure Investigations of Neutral and Charged Ruthenium Bis(β-diketonate) Complexes of Redox-Active Verdazyl Radicals

Stephen D. J. McKinnon,[†] Brian O. Patrick,[‡] A. B. P. Lever,*[,§] and Robin G. Hicks*[,†]

[†]Department of Chemistry, University of Victoria, P.O. Box 3065 STN CSC, Victoria, BC. V8W 3V6, Canada

[‡]Crystallography Laboratory, Department of Chemistry, University of British Columbia, Vancouver, BC, V6T 1Z1, Canada

[§]Department of Chemistry, York University, Toronto, Ontario, M3J 1P3, Canada

Supporting Information

ABSTRACT: The electronic structures of (Vd)Ru(LX)$_2$ complexes (Vd = 1,5-diisopropyl-3-(2-pyridyl)-6-oxoverdazyl radical; LX = acac or hfac) as neutral, cationic, and anionic species have been investigated experimentally and computationally to probe the interplay between the ruthenium ion and the redox-active verdazyl ligand. The cationic complexes were prepared by oxidation of the corresponding neutral species with silver(I) salts. The hfac-based anionic complex was synthesized by reduction of the neutral species with cobaltocene, but the anionic acac analogue could not be prepared. Experimental (X-ray structures, electronic spectra) and computational (TD-DFT (PCM)) studies reveal that the expression of redox activity of the ligand and metal moieties is highly sensitive to the nature of the ancillary ligands on ruthenium.

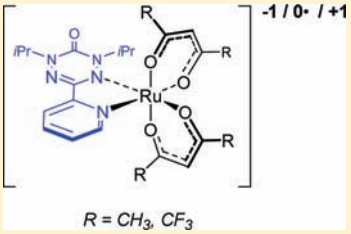

In the hfac series, the cationic, neutral, and anionic complexes can, respectively, be adequately described as Ru(II) complexes of a coordinated verdazyl cation, neutral radical, and anion. However, the more electron-donating acac coligands facilitate a stronger interaction between ruthenium and verdazyl via Ru(d) to Vd(π^*) backbonding which is dependent on the overall charge of the complex and has the net effect of creating a high degree of metal−ligand covalency. Studies on the two cationic complexes reveal further distinctions between the acac- and hfac-containing systems: whereas the former has a significant open-shell singlet contribution to the complex ground state, this open-shell formulation is a minor component of the latter.

INTRODUCTION

Redox-active ligands (RALs) (also known as "noninnocent" ligands[1]) can mimic the properties of transition metals in their ability to adopt (i) more than one redox state and (ii) an open-shell configuration in at least one of their accessible states. As such, RAL complexes have attracted attention because the elucidation of their electronic structure poses special challenges[2] associated with the assignment of metal and ligand oxidation states, electronic coupling, and possible metal−ligand covalency.[3] In addition to long-standing fundamental investigations, there are several examples of RAL complexes in biological systems.[4] More recently, there has been increasing interest in the synthetic applications of RAL complexes:[5] in the past decade, there have been a number of examples in which ligand-centered redox activity contributes directly to stoichiometric or catalytic transformations.[6]

Investigations of RAL complexes have long been dominated by the large family of related ligands comprised of *o*-dithiolenes,[7] *o*-dioxolenes,[8] α-diimines,[9] and mixed-donor and multidentate variants. These ligand subclasses, and other more recently discovered RALs such as mono-[10] and diimino-pyridines,[11] all share a common trait, namely, access to a triad of oxidation states (neutral, anion, and dianion) in which the monoanionic state is paramagnetic. Another distinct set of RALs also exists based on *uncharged* radicals which can be reduced to diamagnetic anions and (in principle) oxidized to closed-shell cations. The redox activity of the ubiquitous small molecules NO and O_2 is a major theme in their coordination (bio)chemistry; among organic radical-based ligands, phenoxyls have been the predominant ligand type whose redox activity has been extensively investigated.[12] Interest in metal−phenoxyl chemistry has been largely inspired by the fungal enzyme galactose oxidase, an alcohol oxidation catalyst whose activity derives from the interplay between a copper ion and a coordinated tyrosyl radical.[13] Catalytic aerobic alcohol oxidation has been demonstrated with other metal−radical complexes, including those based on nitroxides (although these are not well-defined complexes, instead consisting of mixtures of a nitroxide, metal salt or complex, and other reagents[14]) and the recently discovered aminyl radicals,[15] but overall the *chemical* applications of metal−radical redox activity are significantly narrower in scope compared to the more well-known redox active ligands.

Verdazyl radicals (**1**, **2**) are the only organic radicals whose general stability rivals that of the more well-known nitroxides,[16] and their coordination chemistry has been steadily growing since the first metal−verdazyl complexes were reported by Brook.[17] Verdazyls have been successfully coordinated to many different metal ions, including several first row transition metals (Mn(II),[18−21] Co(II),[22,23] Ni(II),[18−22,24] Cu(I),[17,25] Cu(II),[20,26,27] Zn(II)[20,28]),

Received: May 25, 2011
Published: July 19, 2011

ACS Publications © 2011 American Chemical Society

second and third row metals (Cd(II),[28] Hg(II),[28] Ru(II),[29] Pd-(II),[30] Ag(I)[31]), and even lanthanides.[32] However, the redox properties of these complexes have been almost[29] entirely ignored, despite the fact that the general redox activity of free (non-coordinated) verdazyls themselves is reasonably well-established.[16] We recently reported ruthenium(II) complexes **3H** and **3F** of verdazyl derivative **2a** in which redox-activity of the *coordinated* radicals was investigated.[33] Experimental and computational studies indicate that the electron-rich ruthenium center in **3H** is capable of substantial π-donation into the verdazyl π^* singly occupied molecular orbital (SOMO), a phenomenon which can be represented by an additional formulation Ru(III)−Vd(−) in resonance with the conventional Ru(II)−Vd(0) description. This effect is attenuated in **3F** which contains more electron-withdrawing hexafluoroacetylacetonato (hfac) ligands; as such, the ancillary ligands on Ru strongly influence the interplay between Ru and Vd chromophores, leading to tunable metal−ligand noninnocence in the neutral complexes. Analogous issues can arise for the *charged* forms of these complexes (for example, limiting representations of the cations, $\mathbf{3H}^+$ and $\mathbf{3F}^+$, are Ru(III)−Vd(0) or Ru(II)−Vd(+)) whose stability is inferred from the cyclic voltammograms of the neutral species; both **3H** and **3F** possess reversible reduction and oxidation processes, and a second reversible oxidation is evident in the case of **3H**. Herein, we present experimental and computational studies of the electronic structure of ruthenium−verdazyl complexes, with emphasis on understanding the nature of the cationic and anionic species.

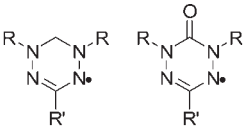

1 **2**

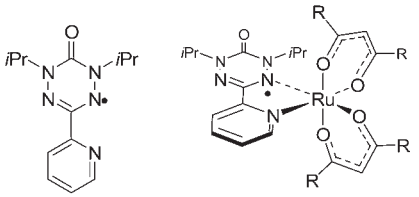

2a **3H** R = CH_3 **3F** R = CF_3

RESULTS AND DISCUSSION

Synthesis and Characterization. Reaction of **2a** with Ru(LX)$_2$(MeCN)$_2$ (LX = acac or hfac) gives the neutral complexes, **3H** and **3F**, respectively, in good yields as deep green crystalline solids.[33] Cyclic voltammetry studies on both complexes reveal chemically and electrochemically reversible oxidation and reduction processes for both, and for **3H** a second oxidation process was also observed.[33] The reversibility associated with all redox processes in the voltammograms prompted us to synthesize cationic and anionic forms of **3H** and **3F**. The cationic species $\mathbf{3H}^+$ and $\mathbf{3F}^+$ were prepared by reactions of the corresponding neutral compounds with silver(I) salts. In the case of **3H**, the oxidant was silver nitrate, and subsequent metathesis with $NaBPh_4$ facilitated the isolation of $\mathbf{3H}^+$ BPh_4^- as a deep red solid. The reaction of **3F** with $AgBF_4$ afforded $\mathbf{3F}^+BF_4^-$ directly as a deep blue material. Syntheses of the anionic forms of the ruthenium−verdazyl complexes were only successful in the case of **3F**, for which the reaction with cobaltocene afforded the salt $CoCp_2^+\mathbf{3F}^-$ as a dark red, air-sensitive material. The corresponding reaction with **3H** did not lead to electron transfer, which is consistent with the much more negative reduction potential of **3H** compared with **3F**. The stronger reducing agent decamethylcobaltocene does react with **3H** but leads to complex and very air-sensitive mixtures, and we were unable to isolate salts of the anion $\mathbf{3H}^-$. This species could, however, be characterized in situ by spectroelectrochemical techniques (vide infra).

Table 1. Carbonyl Stretching Frequencies in Ruthenium−Verdazyl Complexes

compound	ν(CO), cm^{-1}
2a	1686
3H	1664
$\mathbf{3H}^+BPh_4^-$	1712
$CoCp_2^+\mathbf{3F}^-$	1630
3F	1675
$\mathbf{3F}^+BF_4^-$	1752

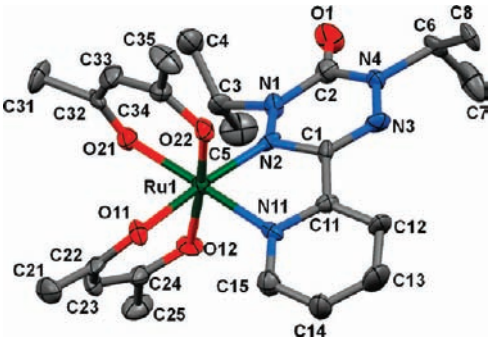

Figure 1. Structure of $\mathbf{3H}^+BPh_4^-$ (50% thermal ellipsoids). Hydrogen atoms, solvent molecule, and the tetraphenylborate anion removed for clarity.

All of the charged complexes (cations and anions) are EPR silent in solution and diamagnetic in the solid state. The carbonyl stretching frequencies in verdazyls of structure **2** and their metal complexes (Table 1) can provide diagnostic information about the electronic structure of the verdazyl complexes. The ν(CO) value of 1686 cm^{-1} for **2a** is typical of 1,5-dialkyl-6-oxoverdazyls and reflects the π-donating capabilities of the two nitrogen atoms flanking the carbonyl group. This affect is attenuated in most first-row metal−verdazyl complexes because the electron-poor metal decreases the donating (to the carbonyl) capabilities of the verdazyl ring; the carbonyl stretching frequency in typical metal−verdazyl complexes rises by 10−25 cm^{-1} relative to that of the free ligand. However, in the neutral Ru complexes **3H** and **3F** ν(CO) is observed at lower frequency, more so in **3H** (1664 cm^{-1}) than in **3F** (1675 cm^{-1}). The changes in ν(CO) upon coordination to Ru are consistent with back-donation, i.e., from Ru(dπ) to verdazyl (π^*), with the more electron-rich Ru(acac)$_2$ fragment being a stronger donor than Ru(hfac)$_2$. Upon oxidation, the ν(CO) frequency increases. For $\mathbf{3H}^+$ the frequency of 1712 cm^{-1} is actually only slightly above the normal regime for *neutral* verdazyl metal complexes but still a little high. For $\mathbf{3F}^+$ the frequency of 1752 cm^{-1} clearly points to a very

electron-deficient verdazyl. The reduced compound $3F^-$ has very low ν(CO) of 1630 cm^{-1}, consistent with reduction taking place predominantly at the ligand.

Structural Characterization. The structures of **3H** and **3F** have been described.[33] Whereas most structural parameters associated with the verdazyl ring usually change very little upon coordination to a metal, coordination to ruthenium leads to significant changes, the most obvious of which is a significant lengthening of the N−N bonds in **3H** and **3F**. The structures of the two cationic complexes $3H^+$ and $3F^+$ (as their BPh_4^- and BF_4^- salts, respectively) and the anion $3F^-$ (as its cobaltocenium salt) are presented in Figures 1−3, and pertinent bond lengths for all species are summarized in Table 2, along with DFT calculated structural parameters (see below). It is instructive to begin with examination of the structural trends in the Ru(hfac)$_2$-based triad (anion, neutral, cation) of complexes. The two N−N bonds in the neutral compound **3F** are slightly longer than those in the uncoordinated radical **2a** which suggest a modest amount of Ru (dπ) to verdazyl (π^*) backbonding.[33] The corresponding cation $3F^+$ and anion $3F^-$ have significantly shorter and longer N−N bonds, respectively, indicative of substantially different charge distributions on the ligand. In the limit that the difference in charge states in $3F^-$, **3F**, and $3F^+$ is accommodated purely by the verdazyl, the radical SOMO occupancy would be 2, 1, and 0 for the anion, neutral, and cation complex, respectively. However, the possibility of changes in the Ru formal oxidation state cannot be ruled out solely based on the structural data, as these would strongly influence the metal's ability to back-donate (or accept). Also noteworthy are the two Ru−N bonds in the triad of related structures—whereas the Ru−N(verdazyl) bond becomes progressively and significantly shorter on passing from anion to neutral and cation, the Ru−N(pyridine) bond does not vary much.

In comparison with **3F**, the more electron-rich Ru(acac)$_2$ fragment in **3H** renders the ruthenium ion a significantly stronger

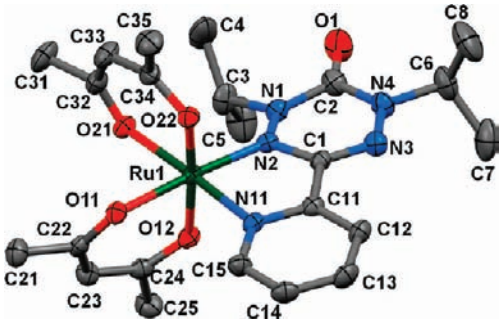

Figure 2. Structure of $3F^+BF_4^-$ (50% thermal ellipsoids). Hydrogen atoms, fluorine atoms, and the tetrafluoroborate anion removed for clarity.

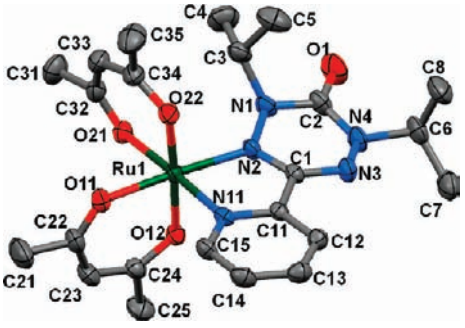

Figure 3. Structure of $CoCp_2^+3F^-$ (30% thermal ellipsoids). Hydrogen atoms, fluorine atoms, and the cobaltocenium cation omitted for clarity.

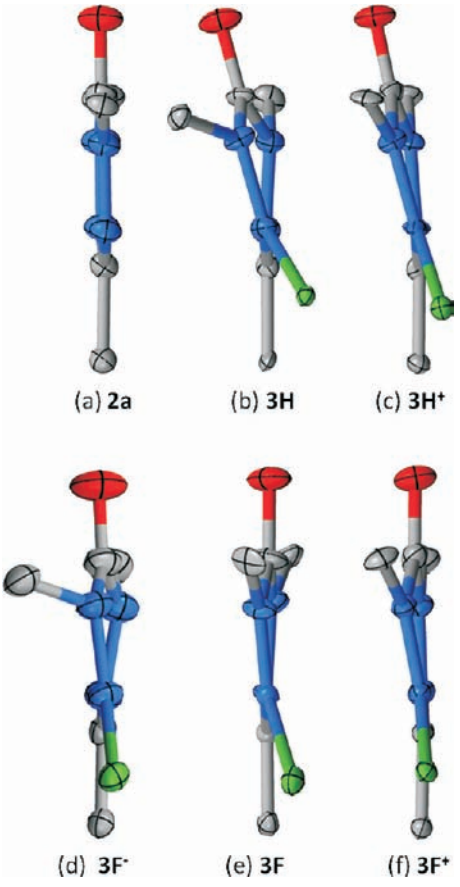

Figure 4. Edge-on view of the verdazyl ring in the structures of (a) **2a**, (b) **3H**, (c) $3H^+$, (d) $3F^-$, (e) **3F**, (f) $3F^+$.

Table 2. Selected Experimental [DFT Calculated[a]] Bond Distances (Å)

bond	2a[26]	$3H^{-b}$	3H[33]	$3H^{+c,d}$	$3F^-$	3F[33]	$3F^{+c}$
N1−N2	1.365(2)	[1.46]	1.448(11) [1.43]	1.397(7) 1.372(7) [1.40]	1.448(3) [1.45]	1.392(2) [1.41]	1.358(3); 1.358(3) [1.37]
N3−N4	1.365(2)	[1.46]	1.387(11) [1.40]	1.341(7) 1.343(7) [1.36]	1.423(3) [1.44]	1.372(5) [1.38]	1.336(3); 1.341(4) [1.34]
C2−O1	1.216(2)	[1.28]	1.241(11) [1.26]	1.198(7) 1.197(7) [1.25]	1.229(3) [1.24]	1.223(5) [1.25]	1.205(4); 1.198(4) [1.24]
N2−Ru	-	[2.11]	1.941(8) [2.02]	1.965(5) 1.988(5) [1.95]	2.0631(19) [2.07]	2.020(3) [2.08]	1.951(2); 1.965(2) [1.99]
N11−Ru	-	[2.05]	2.043(12) [2.06]	2.062(5) 2.055(5) [2.07]	2.0348(19) [2.07]	2.035(3) [2.06]	2.043(2); 2.037(2) [2.06]

[a] DFT B3LYP/LANL2DZ, PCM (dichloromethane). [b] No experimental structure; DFT data only presented. [c] Two molecules in the asymmetric unit. [d] Broken symmetry calculation, vide infra.

π donor, which produces significantly longer N−N bonds in **3H**−particularly the N1−N2 bond adjacent to the ruthenium ion.[33] The cationic complex $\mathbf{3H}^+$ also shows significant N−N bond shortening relative to **3H**. The N−N bonds in the *neutral* **3H** are closest to the corresponding bonds in the *anion* $\mathbf{3F}^-$, and there are analogous similarities in the verdazyl structures in *cationic* $\mathbf{3H}^+$ and *neutral* **3F**. However, the Ru−N(Vd) bond lengths in the cation $\mathbf{3H}^+$ do not seem to fit this picture, as they are *longer* than those in the corresponding neutral species.

The verdazyl ring conformation is also perturbed upon coordination to ruthenium. When not coordinated to a metal, the verdazyl heterocycle is flat (Figure 4a), with the C═O and C1−C11 bonds colinear and the two three-coordinate N atoms (N1 and N4) being trigonal planar. In other metal complexes of bidentate neutral verdazyls, these features are only minimally perturbed; the N2−metal bond is typically tilted from the verdazyl plane slightly (torsion angles 6−10°). In the structure of **3F**, these features are more or less retained, though there is a slight torsional twisting about both N−N bonds. The structure of **3H** reveals more substantial changes to the ring conformation: the ring is no longer planar, the carbonyl group is tilted with respect to the CC bond opposite it, the N2−Ru bond is substantially more twisted from the plane (defined by N2−C1−N3, 20.4°), and the geometry at N1 is not quite trigonal planar (sum of angles = 355.2°). These structural features are present to a much smaller degree in $\mathbf{3H}^+$ and $\mathbf{3F}^+$. In the anion $\mathbf{3F}^-$ the N1 atom is significantly pyramidalized (sum of angles = 344.8°).

Density Functional Theory Analysis. We discuss data for the various charged states (neutral, cation, anion) of the ruthenium−verdazyl complexes based on **3H** and **3F**. In general, the verdazyl ligand is written as Vd if no specific oxidation state is implied or Vd(n) to describe the cationic complex as Vd(+), the neutral species as Vd(0), and the anion as Vd(−). The labels hfac(−) and acac(−) are used for the two β-diketonate ligands. The DFT analysis employed used the B3LYP functional and LANL2DZ basis set which are known to work well with many ruthenium species;[34−38] computation is carried out by deriving a geometry optimized file in a PCM (dichloromethane) in silico environment. We do not use the X-ray structure which may be distorted, to some degree, by crystal packing effects. Key bond lengths are presented in Table 2; a complete list of derived bond distance parameters can be found in the Supporting Information. Indeed there is a satisfactory correspondence between the experimental X-ray data and the geometry optimized distances, assuming doublet spin for **3H** and **3F** and singlet spin states for the other species.

Frontier Molecular Orbital (FMO) Analysis of Neutral Complexes 3H and 3F. We begin with a computational view of the two neutral complexes, **3H** and **3F**. The percentage occupation of the frontier orbitals in these species is illustrated in Figure 5. The SOMO (i.e., the α-HOMO, #131 in **3Hα** and #179 in **3Fα**) is dominantly localized on the Vd ligand but with a significant Ru 4d contribution. There is fairly extensive mixing between ruthenium 4d orbitals with both Vd and acac/hfac(−) MOs with the d orbitals being typically only about 60% pure. Of special interest is the degree and mechanism of charge back-donation to the Vd(n) ligand in these species. We refer to this as π-back-donation, but due to the very low symmetry of these species σ and π are not clearly distinguishable. Considering the **3H** species, the frontier filled α-d orbitals (#128−131) are mixed mostly with the α-HOMO of Vd(0) (α-HOMO, or SOMO, α-#70, of Vd(0)). This does not provide a mechanism for back-donation, and the absence of any significant d contribution to the virtual orbitals α-#132−135 speaks for no significant back-donation via the α-manifold. The SOMO (α-HOMO) is #131 and corresponds with the LUMO (#131) in the β-manifold. The α-LUMO is mainly localized on Vd(0).

While the pattern for the filled orbitals of the **3H** β-manifold looks similar, most crucially, the d orbitals (129,130β) mix not with filled orbitals of Vd(0) but with the *virtual* orbitals of Vd(0), mostly the β-LUMO (β-#70 of Vd(0) with some higher virtual contributions). Back-donation to a ligand L is facilitated mechanistically by the mixing of virtual orbitals of L into the filled orbitals of the complex. Thus, the β-manifold mixing *does* provide a mechanism for back-donation, and this is seen obviously in the significant d orbital contribution to the β-LUMO (#131) (see numerical data in Table 3). Orbital 128β does mix with the filled Vd(0) β-HOMO-2.

The orbital mixing pattern is fundamentally the same for the **3F** species except that π-back-donation to Vd(0), also almost exclusively via the β-manifold, is much smaller. This is clearly a consequence of the electron-withdrawing nature of the fluorine atoms which make hfac(−) a poorer donor to ruthenium. Indeed, there is substantially less 4d−hfac(−) mixing in **3F** compared with 4d−acac(−) mixing in **3H**. The SOMO is α-HOMO #179 corresponding with the β-LUMO #179.

However, the LUMO and LUMO+1 of the **3Fα** manifold are hfac(−) localized. These are the in- and out-of-phase coupled combinations of the π^*-LUMO of the individual hfac(−) ligands (Figure 6). Back donation to hfac(−) is appreciably greater than to Vd(0) as is perceived by the greater d orbital contribution to (α,β) MO #181. Evidence for the noninnocent behavior of α-diketonate ligands has been previously advanced.[39] Similarly, the LUMO+1, +2 of $\mathbf{3F}^+$, and LUMO and LUMO+1 of $\mathbf{3F}^-$ are these π^* hfac(−) localized orbitals. In the **H** series, these π^* orbitals on acac(−) are clearly found as LUMO+2,+3 in $\mathbf{3H}^+$. However in **3Hβ** and $\mathbf{3H}^-$ they are distributed over the three low-lying acac(−) dominated MOs.

Table 3 summarizes the net σ-donation and π-back-donation for all complexes derived from the Frenking charge decomposition analysis (CDA)[40] as extended (ECDA) by Gorelsky.[41,42] The ECDA method provides an approximate value for the net number of electrons transferred by σ-donation and π-back-donation. Table 3 also contains the net transfer of charge from or to the Vd(n) ligand, while Table 4, inter alia, reveals the net charge residing on Vd(n). This latter quantity may not exactly equal the difference between σ-donation and π-back-donation to/from the $Ru(LX)_2$ fragment (LX = acac or hfac) from/to Vd(n) because of polarization effects;[41] however, for the choice of fragments used in this analysis, the *difference* in polarization of the two fragments is close to zero in most cases, and the net charge on Vd(n) does roughly equal the difference between σ-donation and π-back-donation. For **3H** and **3F**, these quantities can be separately assessed for the α- and β-spin manifolds. σ-Donation is, not unexpectedly, roughly the same for both manifolds and indeed roughly the same for both these species. However, as noted above, from the d orbital contribution to the β-LUMO (Figure 5), the π-back-donation in the β-manifold at 0.58 electrons for **3H** is much greater than 0.22 electrons for **3F**, leading to the Vd(0) ligand on **3H** having ca. 0.4 electrons more negative charge than on **3F** (Table 4).

In the case of **3F**, the spin resides predominantly on the Vd(0) ligand, and a description of this species as $(hfac)_2Ru^{II}Vd(0)$ species is reasonable (Table 5). However, in the case of **3H**, the

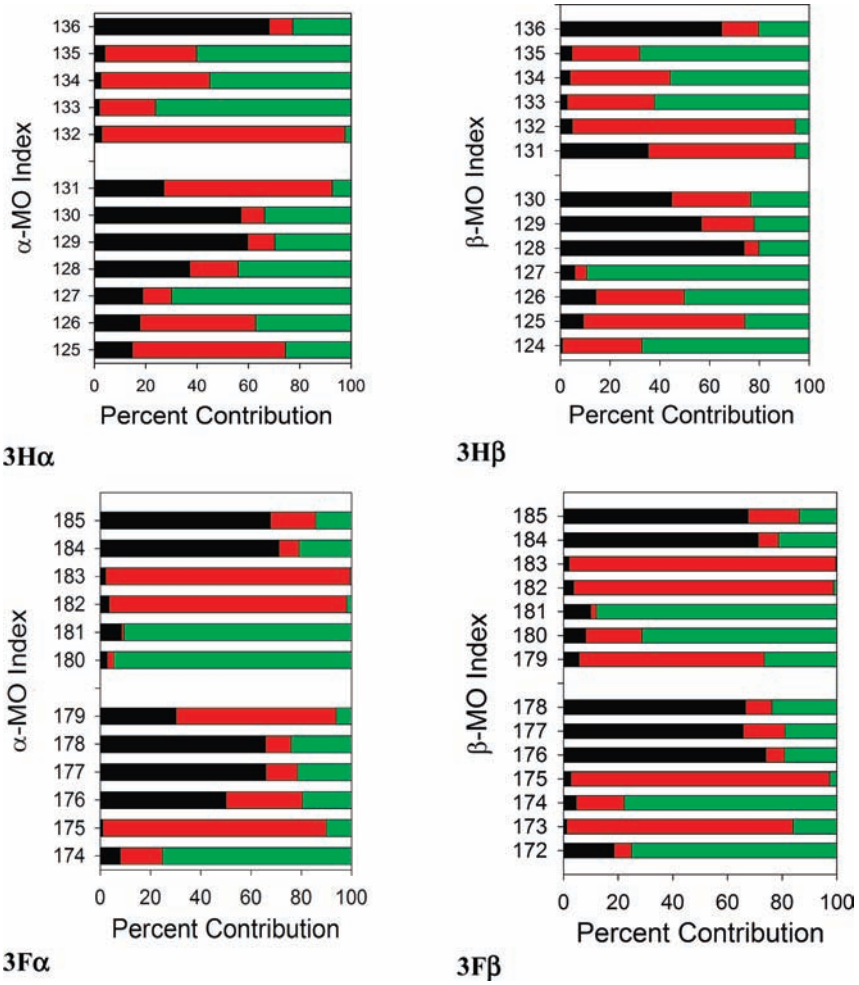

Figure 5. Percentage contributions in the frontier molecular orbitals of **3H** (upper, α and β MOs) and **3F** (lower, α and β MOs). Color code: Ru (black), Vd ligand (red), acac or hfac ligand (green). NB high-lying orbitals with significant d orbital content; e.g., **3Fα** #184,185 are the σ^* orbitals. The largest horizontal white space separates HOMO from LUMO.

Table 3. Net Electrons Transferred, σ-Bonding, and π-Back-Donation (Mulliken)[a]

species	σ-donation from Vd(n) to Ru(LX)$_2$	π-back-donation to Vd(n)	π-back-donation to LX
3F$^-$	0.84	0.19	0.54
3F	0.31α, 0.33β	0.08α, 0.22β	0.18α,0.19β
3F$^+$	0.64	0.68	0.29
3H$^-$	0.61	0.26	0.30
3H	0.30α, 0.30β	0.10α, 0.58β	0.13α,0.14β
3H$^+$	0.63	1.08	0.31
3H$^+$ **(BS)**[b]	0.33α,0.59β[c]	0.22α,0.10β[c]	0.16α,0.16β

[a] LX = acac or hfac. Data are relative to the formal charge of the Vd species, i.e., +1 for Vd(+), 0 for Vd, and −1 for Vd(−). [b] Data relative to Vd(0). [c] Approximate values as the polarization term for the β-electrons is not insignificant, namely, 0.08 electrons from Ru(acac)$_2$ to Vd.

spin is almost evenly distributed between ruthenium and Vd(0) as a result of the extensive back-donation in the β-manifold which transfers some net β-spin to Vd(0) leaving net α-spin on ruthenium. Thus, this species is probably best understood as (acac)$_2$Ru^{II}Vd(0) mixed with a substantial contribution from

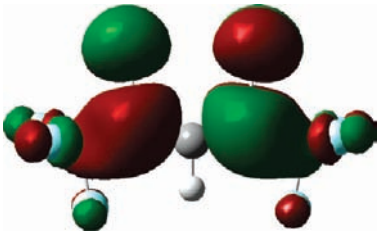

Figure 6. hfac(−) π^*-LUMO. The C═O bonds point up the page.

(acac)$_2$Ru^{III}Vd(−). Since back-donation is much smaller in **3F**, the net spin residing on ruthenium is also much smaller. These data are consistent with the previously reported electron paramagnetic resonance data for these complexes,[33] wherein **3F** shows a primarily free radical spectrum arising from the radical Vd(0) ligand while **3H** shows significant additional coupling to ruthenium.

Since the Vd(0) ligand is formally neutral, one might expect that the σ-donation to a metal center would lead to a net positive charge on this ligand, but in fact there is a net negative charge, albeit small, in **3H**, due to the considerable π-back-donation. This is, of course, another manifestation of the Ru^{III}Vd(−)

Table 4. Mulliken Net Charges and Mayer Bond Orders between Fragments

	net Mulliken charge				Mayer bond order		
	Ru	Vd[a]	LX[b]	Ru^{II}—Vd(n)[c]	((LX)Ru^{II})—Vd	Ru^{II}—LX[d]	Vd(n) —LX[e]
$3F^-$	0.52	−0.38	−1.14	1.18	1.44	2.74	0.26
3F	0.51	0.36	−0.87	0.52α, 0.73β	0.61α, 0.84β	1.27α, 1.27β	0.09α, 0.11β
$3F^+$	0.61	0.97	−0.58	1.70	2.00	2.44	0.31
$3H^-$	0.45	−0.67	−0.78	1.25	1.44	2.50	0.20
3H	0.54	−0.04	−0.50	0.53α, 0.97β	0.64α, 0.07_Sβ	1.25α, 1.28β	0.11α,0.15_Sβ
$3H^+$	0.63	0.54	−0.17	1.74	2.18	2.66	0.44
$3H^+$ (BS)	0.65	0.53	−0.18	0.68α, 0.73β	0.83_Sα, 0.91β	1.26α, 1.47_Sβ	0.15α, 0.18β

[a] The Mulliken charges residing on the pyridine rings of the Vd(n) ligand are +0.19, +0.31, and +0.46 electrons on $3F^-$, **3F**, and $3F^+$ and −0.14, +0.20_S, and +0.36 electrons on $3H^-$, **3H**, and $3H^+$. [b] LX = acac or Hfac. [c] Between Ru and Vd ligands. [d] Between Ru and acac/hfac ligands. [e] Between Vd and acac/hfac ligands.

Table 5. Mulliken Spin Densities (DFT, PCM (Dichloromethane))

species (spin state)	Ru	LX[a]	Vd(n)
3H (^{2}**Γ**)	0.43	0.02	0.56
3F (^{2}**Γ**)	0.12	0	0.89
$3H^+$ (^{1}**Γ**, BS)	0.57	0.13	−0.70

[a] LX = acac or hfac.

contribution to the ground state. Figure 7 shows the SOMO of **3H** and the computed spin density distribution residing on both Vd(0) and Ru. We defer analysis of internal Vd bond orders until the oxidized and reduced species are introduced.

Fragment Molecular Orbital (FMO) Analysis of Cationic ($3H^+$ and $3F^+$) and Anionic ($3H^-$ and $3F^-$) Complexes. The anions are formed by adding an electron to the SOMO of the Vd(0) ligand to form a closed-shell Vd(−) donor, thus they are diamagnetic, *formally* Ru^{II}Vd(−), species. Mixing of Vd orbitals with metal d orbitals in the anions is not very extensive aside from some delocalization of d orbital density over the Vd(−) HOMO, #131 ($3H^-$) and #179 ($3F^-$). There is no significant back-donation to Vd(−) as indicated by the very small d orbital participation in the LUMO, LUMO+1, etc. (Figure 8). σ-Donation from Vd(−) is the same for both **3H** and $3H^-$ but substantially greater for $3F^-$ relative to **3F** (Table 3). This arises because of the electron attracting power of the hfac(−) ligand which enjoys a much more negative charge in $3F^-$ than in **3F** (Table 3) at the expense of Vd(−); i.e.. the charge is transferred via σ-donation to Ru and back-donation to hfac(−). This is seen by comparing the data in the final column of Table 3 showing the considerable increase in net charge transfer from Vd(−) to hfac(−) in $3F^-$ relative to **3F** compared with that in column 2 of Table 4, showing that the charge on Ru is essentially the same in these two species. The effect is similar but muted in the **3H** and $3H^-$ pair. The 4d filled orbitals in $3F^-$ (#176−178) are all fairly pure (>60%) and only slightly mixed with Vd(−) and hfac(−). The same is true for $3H^-$ except for one d orbital which mixes fairly extensively to form a bonding/antibonding pair (#128 and 131) with the Vd(−) HOMO.

The SOMO of each of the neutral complexes lies mostly on Vd(0) (Figure 5), and it is the electron in this orbital which is lost to make the diamagnetic cations. The LUMO of Vd(+) (which was the SOMO of Vd) is mixed into frontier filled orbitals of *both* $3H^+$ (#130, 129, 127) and $3F^+$ (#178, 177, 174), providing a

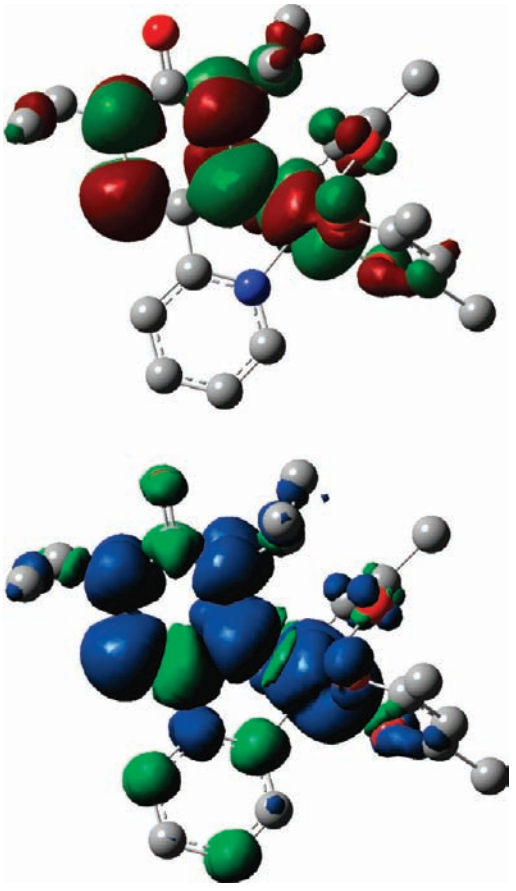

Figure 7. SOMO (top) and Mulliken spin density (bottom) of **3H**. Hydrogen atoms omitted for clarity.

mechanism for back-donation which is reflected in the significant d orbital contribution to the LUMOs (#131 and 179, respectively) (Figure 8). Table 3 illustrates that, again, σ-donation is unaffected (**3H** vs $3H^+$), but π-back-donation is much greater in $3H^+$, obviously because it is a positively charged ligand. It is much more dramatic in $3H^+$ than $3F^+$ because the hfac(−) ligand in the latter suppresses back-donation to Vd(+) (Table 4). Note that the large contribution of Vd(+) to #175 of $3F^+$ is not from the Vd(+) LUMO but primarily from the Vd(+) HOMO-1. It may seem curious that the d orbital mixing in these cations,

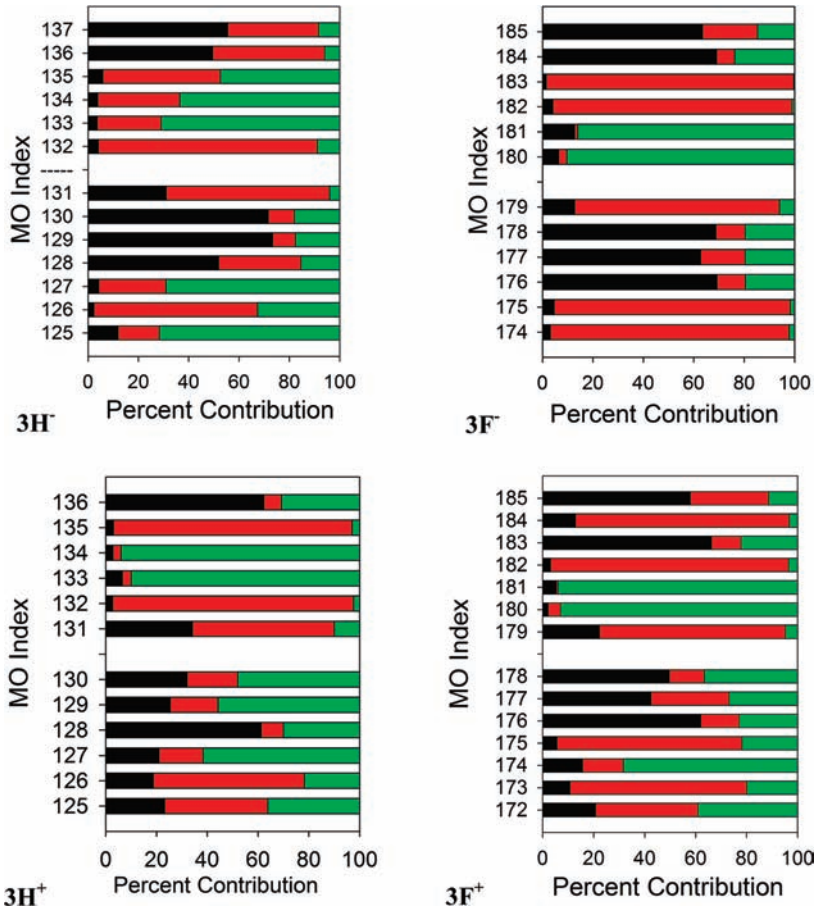

Figure 8. Percentage contribution in the frontier molecular orbitals of the (upper) anions $3H^-$ and $3F^-$ and (lower) cations $3H^+$ and $3F^+$. All species are spin singlets. Color code: Ru (black), Vd (red), acac(−) or hfac(−) (green).

predominantly with acac/hfac(−) molecular orbitals, is substantially greater than in the neutrals or anions, especially for $3H^+$ where only one d orbital has purity exceeding 40% (#128). There are no orbitals lying below #125, with significant d content. Mixing is also substantial, but not quite so dramatic, in $3F^+$. One can observe that the mixing has not increased substantially with the Vd(+) ligand, versus Vd(−). Indeed, these acac/hfac(−) ligands have substantial π-acceptor character. The positive charge on Vd(+) causes these diketonate ligands to be much stronger donors, to form stronger covalent bonds with ruthenium. This then leads to an analysis of bond orders.

Bond Lengths and Interatomic and Interfragment Bond Orders. X-ray crystallographic data are available for all the species except $3H^-$. The Vd(n) fragment contains two N−N bonds whose bond lengths are very sensitive to electronic structure. In the SOMO of Vd(0), a nodal plane passes through each N−N bond.[43] Thus, occupation of that orbital should decrease the bond order of both N−N bonds. Indeed, Table 2 shows that the N−N bond lengths lengthen as we pass from $3F^+$ and $3H^+$ (with no electrons in that orbital) to **3F** and **3H** (one electron) to $3F^-$ (two electrons). The DFT-derived bond orders (Table 4) nicely follow the same trend with the strongest/shortest bonds for the $3F^+$ and $3H^+$ species.

The Ru−N bond lengths and individual Ru−N bond orders are more intriguing. First, it should be recognized (see footnote to Table 4) that, for the anions, the negative charge (Mulliken)[44,45] resides mostly on the tetrazine ring rather than the pyridine moiety of the Vd(−) ligand. For the cations, the positive charge is evenly distributed over both rings for $3F^+$ and is mainly on the pyridine ring for $3H^+$. The bond lengths become shorter, i.e., bonds become stronger, from $3F^-$ to $3F^+$. The Ru−N_2 bond orders to the tetrazine ring show the largest variation (Table 6) with only a small spread in the Ru−N_{11}(pyridine) bond orders. The variation in Ru−N_2 bond order is slightly irregular, but the values are clearly largest for $3H^+$ and $3F^+$. This is somewhat counterintuitive since we are moving from a negatively charged donor ligand, Vd(−), to a positively charged one, Vd(+). The increased bond order must then be attributed to the substantial increase in π-back-donation available to the $3F^+$ and especially $3H^+$ species, the latter having the largest back-donation and the

Table 6. Selected Mayer Bond Orders[a]

species	N_3-N_4	N_1-N_2	Ru−N_2	Ru−N_{11}	Ru−$O(N_2)$[b]
$3F^-$	0.83	0.85	0.50	0.47	0.49
3F	0.97	0.98	0.47	0.49	0.53
$3F^+$	1.08	0.99	0.67	0.51	0.54
$3H^-$	0.81	0.84	0.44	0.49	0.49
3H	0.89	0.88	0.54	0.45	0.54
$3H^+$	0.99	0.90	0.79	0.44	0.59_5
$3H^+$ **BS**	1.00_5	0.95	0.63	0.45	0.60_5

[a] DFT B3LYP/LANL2DZ, PCM (dichloromethane, DCM). [b] Ru−O_{11} *trans* to Ru−N_2.

Table 7. Natural Population Analysis Distribution of Charge on Fragments (Electronic Charge) (DFT)[a]

species	NPA charge on Ru	NPA charge on Vd(n)	NPA charge on LX	NPA charge on [Ru(LX)$_2$][b]
3F$^-$	0.52	−0.27	−1.27	−0.75
3F	0.51	0.55	−1.04	−0.53
3F$^+$	0.58	1.12	−0.78	−0.20
3H$^-$	0.47	−0.50	−0.96	−0.49
3H	0.55	0.18	−0.74	−0.19
3H$^+$	0.62	0.82	−0.44	0.18
BS	0.66	0.77	−0.43	0.23

[a] LX = acac or hfac. Calculated using Gaussian 09 B.01, PCM, DCM. [b] Sum of column 2 and column 4.

largest bond order. Curiously, though, the experimental Ru−N_{11} bond length for **3H**$^+$ is slightly longer than for **3H**. The DFT calculated bond lengths show the expected trend, **3H** (2.02 Å) and **3H**$^+$ (1.95 Å), so the anomaly in the X-ray distance may arise through packing phenomena.

The Mayer bond orders[46] (Table 4) comprise the *total* bond order between defined fragments of the molecule, specifically between Ru and the Vd(n) fragment, between Ru(acac/hfac-(−))$_2$ and Vd(n) fragments, and between Ru and acac/hfac(−). The first two bond orders increase from the Vd(−) to Vd(+) in parallel with the increasing interaction between Ru and Vd(n). The difference between the numbers in the first two Mayer bond order columns is, in effect, a bond order between the Vd(n) and acac/hfac(−) ligands.

Finally, in this section, note that the charge of ruthenium is roughly constant throughout the series in accord with the Pauling Electroneutrality Principle.[47] The charge on Vd(n) changes quite dramatically, consistent with passing from formally Vd(−) to formally Vd(+). The most interesting observation is the very large change of the net charge on the acetylacetonate ligand (both acac(−) and hfac(−)) with change of oxidation state of Vd(n) (Table 4). Thus, as one and two electrons are formally added to Vd(+), much of the charge is shifted to the acac/hfac(−) ligands.

Natural Population Analysis (NPA). We comment briefly on the Natural Population Analysis[48] distribution of charge on fragments shown in Table 7. The Mulliken and NPA charges on the Vd(n) fragment are almost identical, within 0.1e. The NPA charge on Ru is ca. 0.3−0.4 more positive than the Mulliken value, but the trend with oxidation state is the same. We again see the large shift in charge to the acac/hfac(−) moiety as we proceed from Vd(+) to Vd(−) with the NPA charges on acac/hfac(−) being about 0.4−0.5 electrons more negative than the Mulliken values. The NPA net sum on the [Ru(acac/hfac)$_2$] unit is also shown and will be commented on below. Thus, the NPA method paints a very similar picture to the MPA method discussed below.

Electron Occupation of the Vd(0) SOMO. Greater insight can be obtained by evaluating as a function of "n", the MPA electron occupation within the complexes, of the Vd(n) MO #70 which, in Vd(0), contains the odd unpaired α-electron. Table 8 shows that the occupation of this orbital is close to 2.0 electrons in **3F**$^-$ and **3H**$^-$ as expected for the Ru^{II}Vd(−) species. The neutral species **3H** and **3F** contain one α-electron with additional back-donation of β-electron density indicating, as noted above, that the species contains a resonance contribution of Ru^{III}Vd-(−), which is more important in **3H** than in **3F**.

Table 8. Occupation (MPA) of the HOMO and LUMO of the Vd(n) Fragment and NPA Configuration of Ru 4d Orbitals (DFT, PCM (DCM))[a]

	HOMO	LUMO	NPA d^n configuration n
3F$^-$	1.86 (#70)	0.07 (#71)	6.88
3F	0.99α (#70), 0.87β (#69)	0.05α (#71), 0.23β (#70)	3.49α, 3.39β
3F$^+$	1.71 (#69)	0.51 (#70)	6.80
3H$^-$	1.97 (#70)	0.15 (#71)	6.92
3H	1.0α (#70), 0.88β (#69)	0.06α (#71), 0.44β (#70)	3.59α, 3.23β
3H$^+$	1.75 (#69)	0.89 (#70)	6.73
BS	0.80_5α (#70)[b], 0.86β (#69)	0.03α (#71), 0.12β (#70)	6.69

[a] The LUMO of Vd(+) and SOMO of Vd is #70. [b] 0.86α (#69).

While #70 is nominally empty in the cations, mixing of this virtual orbital with filled orbitals of the complex contributes half a β-electron in **3F**$^+$ and nearly 0.9 β-electrons in **3H**$^+$. Thus, oxidation of **3F** and **3H** leads to a species which can be described as a resonance hybrid of (LX)$_2$$Ru^{II}$Vd(+) and (LX)$_2$$Ru^{III}$Vd(0) (LX = acac, hfac) with the latter being much more important in **3H**$^+$ than in **3F**$^+$. The natural population configuration of the ruthenium 4d levels, which is also shown in Table 8, decreases from the anion to the cation as the Ru^{III} component increases. Thus, the first electrochemical oxidation of **3H** is substantially ruthenium-based.

Singlet Diradical, Broken Symmetry, Solutions for Cations 3H$^+$ and 3F$^+$. The cationic complexes **3H**$^+$ and **3F**$^+$, formally Ru^{II}Vd(+) species, have a significant contribution from a Ru^{III}Vd(0) resonance form. Since the Vd(+) species are diamagnetic, the (LX)$_2$$Ru^{III}$Vd(0) formulation involves a simple Ru−Vd covalent bond but can be interpreted in terms of strong antiferromagnetic coupling between the odd electron formally in d^5 Ru^{III} and the "radical" electron of Vd(0). However, this restricted spin singlet state may be unstable with respect to an unrestricted spin "singlet diradical" configuration. The closed-shell (restricted spin, RHF) singlet model comprises a pair of electrons, of opposite spin, in one molecular orbital. The singlet diradical consists of a pair of antiferromagnetically coupled electrons, in different orbitals, which give rise to three singlet states and one triplet state which may, if weakly coupled, have very similar energies.[49,50] The rigorous application of standard Hartree−Fock and DFT methods to such a system requires a multiconfigurational ground state and is computationally very demanding. A characteristic of the singlet diradical is the spin expectation $<S^2>$ differing from zero (Table 9).[27] Singlet diradicals are regarded as linear combinations of singlet and triplet wave functions[51] and should therefore have $<S^2>$ between 0 and 1.[52] The closer to 1, the greater is the diradical character. For a pure closed-shell singlet. $<S^2>$ would be zero. Noodleman[53] introduced the "*broken symmetry*" (**BS**) formalism based on unrestricted Hartree−Fock (UHF) wave functions allowing the α- and β-electron to be placed in different orbitals in different parts of the molecule. This formalism mimics the singlet diradical. The **BS** orbitals are not spatially orthogonal and are not symmetry adapted to the point group of the molecule, hence the term broken symmetry. Importantly, the Noodleman approach allows this situation to be approximated by a *single* determinant using UHF wave functions. This method is commonly used to calculate antiferromagnetic coupling (exchange) constants.[54] This formalism, especially in the field of noninnocent ligand

Table 9. SCF Energies of $(LX)_2RuVd(+)$ Species: Gaussian 09 Calculation, PCM with Dichloromethane (Hartree)[a,b]

species	$L_2Ru^{II}Vd(+)$ $S = 0$	$L_2Ru^{III}Vd(0)$ $S = 1$	$L_2Ru^{III}Vd(0)$ $S = 0$ **BS**	$<S^2>$ value of **BS** state
$\mathbf{3H}^+$	−1639.20234	−1639.19471	−1639.20617	0.5498
$\mathbf{3F}^+$	−2830.08116	−2830.06126	−2830.08147	0.1806

[a] LX = acac, hfac. [b] Restricted spin singlet optimized geometries.

chemistry, often provides a UHF description of a singlet state, with an energy more negative than the restricted solution. The broken symmetry solution is detected through use of the Gaussian DFT STABLE=OPT keyword which will seek out such potential lower energy **BS** ground states. Previous work by Neese, Wieghardt, and other groups has revealed that **BS** ground state contributions are fairly common with noninnocent ligand complexes.[55,56] The reader is directed to these publications for a thorough analysis of broken symmetry solutions.

Using Gaussian 09 and the PCM model with dichloromethane, an instability in the restricted solution was found with both $\mathbf{3F}^+$ and $\mathbf{3H}^+$ (Table 9). Using the restricted spin optimized geometries, a broken symmetry, unrestricted spin, singlet diradical ground state was more stable in both $\mathbf{3F}^+$ and $\mathbf{3H}^+$ than the restricted spin solution discussed above. The corresponding spin triplet ($S = 1$) energy, also of the singlet spin geometry, is *less stable* than either the restricted solution or the **BS** solution. An $<S^2>$ value of 0.58 for $\mathbf{3H}^+$ reveals a substantial (58%) singlet diradical contribution to the ground state, and on this basis, $\mathbf{3H}^+$ is more clearly a singlet diradical than $\mathbf{3F}^+$. Indeed, we show below that the time-dependent DFT predicted spectrum of the **BS** ground state of $\mathbf{3H}^+$ is a slightly better fit to the experimental spectrum than the spectrum derived from the closed-shell restricted spin ground state. The **BS** solution for the $\mathbf{3F}^+$ complex evidently makes a much smaller contribution ($<S^2>$ close to zero), and its electronic spectrum is no improvement over that of the closed-shell solution. We have also noted that the $(LX)_2Ru^{III}Vd(0)$ component is much smaller for $\mathbf{3F}^+$ than for $\mathbf{3H}^+$. Thus, we will not consider the **BS** solution for $\mathbf{3F}^+$ any further.

It is interesting to learn what the electronic description of this **BS** state is. Clearly we would expect it to be $(LX)_2Ru^{III}Vd(0)$ with spins localized on ruthenium and on the Vd ligand. There are a variety of ways to identify the "magnetic orbitals" that contain the two antiferromagnetically coupled electrons. One might expect them to be the α- and β-HOMO of the system, but this is not necessarily the case. Neese points out[51] that the α- and β-orbitals of a singlet diradical can be identified by looking at the MOs and observing which α- and which β-orbital lack a corresponding partner. In this very low symmetry system, mixing is so considerable that it is not easy to make this assignment. A much better procedure is to carry out the "corresponding orbital transformation" (COT).[52,57] In this procedure, the α- and β-orbital manifolds are subjected to a unitary transformation so that each α-orbital overlaps just one β-orbital. This, in general, will give rise to three possible conditions: (i) closed-shell MOs where the α- and β-orbitals overlap with an overlap integral $S_{\alpha\beta} > 0.99$, (ii) orbitals having no partner, i.e., unpaired electrons, and, importantly, (iii) MOs where the α- and β-orbitals weakly overlap with an overlap integral of $S_{\alpha\beta} < 0.99$, so-called "magnetic orbitals" which comprise the "singlet diradical" and where the electrons are weakly antiferromagnetically coupled. After carrying out this procedure, we discover, for $\mathbf{3H}^+$, one αβ pair with $S_{\alpha\beta} < 1$. They are indeed the α and β HOMOs #130 (Figure 9) with $S_{\alpha\beta} = 0.68$.

One can derive an approximate value for the singlet−triplet splitting, J, energy, linking the singlet diradical to the corresponding spin triplet diradical, from eq 1[56,58,59]

$$J = -[E(\mathbf{BS}) - E(\mathrm{T})]/[<S^2>_{\mathrm{T}} - <S^2>_{\mathrm{BS}}] = \text{ca. } -1700\ \mathrm{cm}^{-1} \quad (1)$$

where $E(\mathbf{BS})$ and $E(\mathrm{T})$ are the SCF energies of the broken symmetry singlet and spin triplet, respectively (Table 9), and $<S^2>$ are the relevant spin expectation values. This value of J is typical of values found for other noninnocent radical ligand **BS** ground states.[49,56,60] It is sufficiently large that the spin triplet state is not thermally accessible.

One can derive a singlet diradical, broken symmetry, percentage contribution to the description of the ground state of this complex using eq 2, which is essentially the same as that derived from $<S^2>$[59]

$$\%\mathbf{BS} = 100(1 + |S_{\alpha\beta}|)(1 - |S_{\alpha\beta}|) \approx 54\% \quad (2)$$

The singlet spin (restricted) optimized geometry was used to explore the singlet diradical configuration, but one might question whether the optimized structure of the triplet spin $\mathbf{3H}^+$ would be a better choice. Indeed, the DFT optimized triplet spin geometry of $\mathbf{3H}^+$ is more stable (SCF = E(G09, UB3LYP, PCM DCM) = −1639.207 054 56 hartree) than the singlet spin geometry (SCF = E(G09, UB3LYP, PCM DCM) = −1639.202 772 70 hartree). However, this is a situation where DFT provides energy for an open-shell calculation which is rather too negative since experimentally this $\mathbf{3H}^+$ species is known to be diamagnetic. More seriously however, this triplet spin structure possesses an unrealistically long Ru−N_2 bond of 2.12 Å. This structure does yield a singlet diradical which is even more stable (SCF = E(G09, UB3LYP, PCM (DCM)) = −1639.208 275 0 hartree) than the triplet (with $<S^2> = 0.9508$, $S_{ab} = 0.28$); however, given the poor fit to the crystal structure, this solution is not acceptable, and we prefer the singlet diradical based on the singlet spin geometry.

We ascribed, above, the delocalization of charge in $\mathbf{3H}^+$, via π-back-donation, to a resonance mix of two closed-shell extreme models, $[(acac)_2Ru^{II}Vd(+)]^+$ and $[(acac)_2Ru^{III}Vd(0)]^+$. We can now see that there is another contribution which specifically differs from either of these, an open-shell, singlet diradical $[(acac)_2Ru^{III}Vd(0)]^+$ where the spins are strongly coupled. The description of this state using conventional oxidation state language is not so clear. Figure 9 shows these magnetic orbitals with the percentage breakdown over the molecule noted in the legend. The α-electron is clearly associated with the $[(acac)_2Ru^{III}]^+$ fragment, but the β-electron is in an orbital fairly evenly spread over the entire molecule. We note, however, that this is a broken symmetry approximation to reality since a spin singlet does have to have zero spin at all points in the molecule. The percentage contributions to the α- and β-manifolds are shown in Figure 10.

Considering the data in Table 8, the occupation of the Vd orbital #70 provides useful information. Thus, the closed-shell

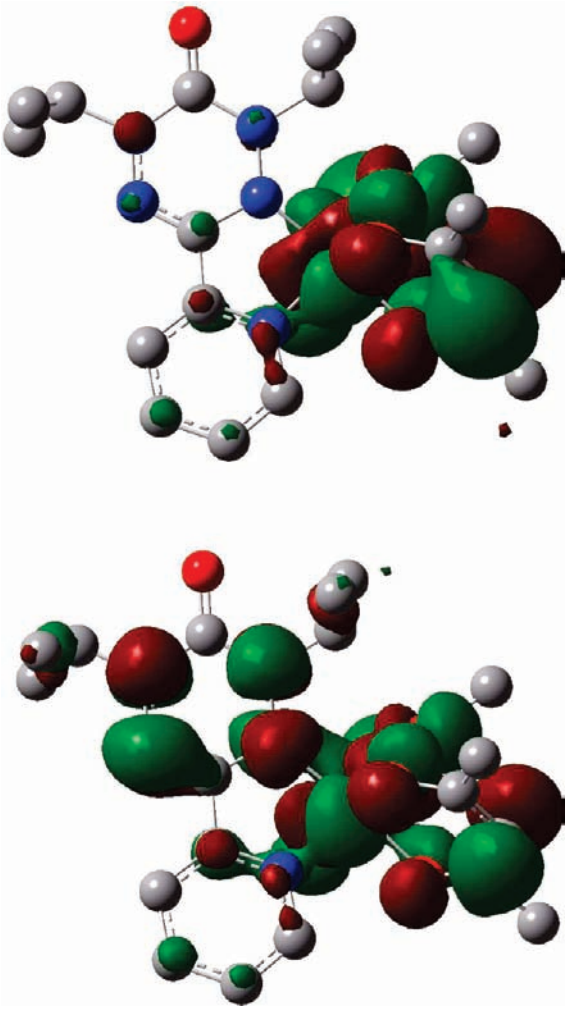

Figure 9. Broken symmetry, singlet diradical COT orbitals: α #130 (top, 3.9% Vd, 64.8% acac, 31.3% Ru) and β #130 (bottom, 35.3% Vd, 31.4% acac, 33.3% Ru). DFT unrestricted spin. Hydrogen atoms omitted for clarity.

version of $\mathbf{3H}^+$ reveals just under one electron in this orbital which implies then $[(acac_2)Ru^{III}Vd(0)]^+$ as a major contributor but, of course, with no net spin on either Ru or Vd. The **BS** solution also places close to one α-electron in #70, but this is then only partially coupled to Ru through the singlet diradical mechanism. The net spin of 0.57 (Table 5) on Ru (+0.7 on $[Ru(acac)_2]^+$) suggests also that $[(acac)_2Ru^{III}Vd(0)]^+$ is a major contributor to the structure but now with a different electronic structure leaving net spin on both Ru and Vd. The rather better agreement between the predicted and experimental electronic spectrum using this **BS** solution, and the fact that it is of lower SCF energy than the restricted singlet, provides the argument for accepting the **BS** solution as a better portrayal of this molecule than the closed-shell version.

Table 4 reveals that the Mayer bond orders for both Ru−Vd and $(acac)_2$Ru−Vd are smaller for the **BS** state than for the closed-shell state, and this may be simply related to the weaker bonding between the Ru^{III} and Vd(0) radicals in the former relative to the latter. However the Mulliken (and NPA) charges appear essentially unchanged between the two $\mathbf{3H}^+$ states. The $\mathbf{3H}^+$ species has the most positive net charge on this fragment of all the species (Table 4), somewhat more so than in $\mathbf{3F}^+$, in keeping with our understanding that $\mathbf{3H}^+$ contains primarily Ru^{III}.

Electronic Spectra. The electronic spectra of this series of complexes are amazingly rich as a consequence of the changing formal oxidation state of the verdazyl ligand. The experimental spectroscopic data, along with TD-DFT calculated spectra and assignments for the transitions, are provided (Table 10) up to approximately 30 000 cm^{-1} (see Supporting Information for complete data set). The net charge on the Vd and acac(−) ligands varies over wide extremes as we proceed from cation (Vd(+)) to neutral (Vd(0)) to anionic (Vd(−)) species. We can expect to observe both 4d to Vd(n) and 4d to acac(−) MLCT transitions. Given that Ru is a low spin $(t_{2g})^6$ metal, there will formally be three 4d → L MLCT transitions, for each of Vd(n) and acac/Hfac, but only transitions from the specific d orbital that has π-symmetry with respect to the acceptor π^* orbital of the ligand can be intense.[61] Interligand processes can be expected; either Vd(n) to acac/Hfac or acac/Hfac to Vd(n) may be accessible in the visible region depending on the formal oxidation state of Vd. In principle, there can be many of these since the excited electron may originate from several different frontier filled orbitals with intensities depending on overlap. The lowest-energy MLCT and LLCT transitions to Vd(+) and Vd(0) will terminate on the lowest π^* orbital of Vd(+), but transitions to Vd(−) will terminate on the LUMO+1 of Vd(+) and so may appear at substantially higher energy. Transitions originating from Vd will obviously be of higher energy for Vd(+) than for Vd(−). Internal $\pi-\pi^*$ transitions within Vd(n) and acac/Hfac will also be observed. It is fortunate that TD-DFT works very effectively to reproduce the major features of the electronic spectra of all the species and hence provides assignments. All of the transition types listed above are observed, although some are very weak and hidden under other stronger bands. Excellent fits are generally achieved through the spectrum from the low-energy, NIR bands to high-energy very intense transitions near 35 000 cm^{-1}; indeed, for all the species, overall agreement between theory and experiment is very good to excellent. The NIR bands usually arise from one or, sometimes, two transitions to well-defined excited states, generally arising from HOMO to LUMO. On the other hand, the intense UV absorption arises from a plethora of excited states, most of which comprise small contributions from many MO transitions (see Supporting Information). It is remarkable that despite the complexity of this region of the electronic spectra the TD-DFT calculation reproduces the peak energy almost exactly. One therefore has confidence in the resulting analysis even if one cannot assign the higher-energy absorption to any single simple excitation.

The experimental and calculated spectra of the neutral species **3H** and **3F** are presented in Figure 11.

In these open-shell species, the α- and β-manifolds must be considered separately. In **3H** the LUMO of the α-manifold is almost pure Vd, while the β-LUMO is a mix of 4d and Vd (vide supra). Thus, the weak NIR band near 7000 cm^{-1} (Figure 11, left) is MLCT to Vd(0) from the β-manifold with some $\pi-\pi^*$ Vd (0) character. The next low-energy band is the inverse, in the α-manifold, mostly $\pi-\pi^*$ Vd(0) with some contribution from Ru 4d → Vd(0) MLCT. A broad ill-resolved experimental band maximizing at ca. 27 300 cm^{-1} comprises a large number of predicted transitions. In the UV, there is a well-developed experimental peak at 36 230 cm^{-1} which is dramatically well represented by the predicted TD-DFT summation of multiple transitions in that region.

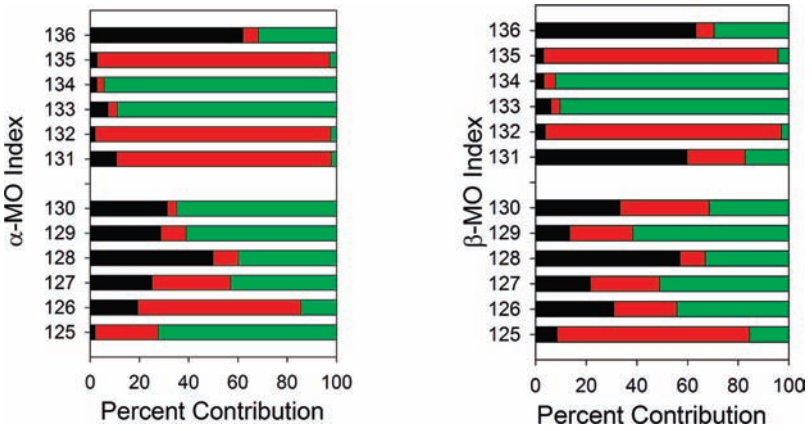

Figure 10. Percentage contribution in the frontier molecular orbitals of the unrestricted spin **BS** $3H^+$ (left, α-manifold; right, β-manifold). Color code: Ru (black), Vd (red), acac(−) (green). The magnetic orbitals are #130αβ.

Turning to **3F**, the LUMO and LUMO+1 in the α-manifold are almost pure hfac(−) π^*, being the in- and out-of-phase coupled π^* level of each independent hfac(−) ligand. The LUMO of the β-manifold is mostly Vd π^*. In this system, there are no expected transitions below 10 000 cm^{-1}. The first excited state predicted at 12 100 cm^{-1} has an oscillator strength of 0.0002 and is an admixture of many small contributions but mostly MLCT to both ligands. The subsequent, weak, predicted transitions are a mix of LLCT from Vd to hfac(−) and MLCT to both ligands. Stronger MLCT to hfac(−) and to Vd occur experimentally near 23 000 cm^{-1}. The first and very weak hfac(−) to Vd LLCT corresponds with very weak absorption near 29 000 cm^{-1}. Maximum experimental absorption near 36 000 cm^{-1} is again well predicted by theory.

The spectra of the cations $3H^+$ and $3F^+$ are displayed in Figure 12. Details are shown in the Supporting Information. For $3H^+$ (**BS** predicted spectrum, Figure 12, red trace) the HOMO to LUMO transition in the NIR region and the nearby weaker transition (ca. 12 000 cm^{-1}) are both accurately predicted by TD-DFT and are a mix of MLCT $Ru^{II} \rightarrow$ Vd and LLCT acac(−) → Vd transitions. The three stronger bands predicted in the 15 000−22 500 cm^{-1} region are a mix of LLCT acac(−) → Vd and internal Vd transitions but with a significant contribution from acac(−) → Ru^{III} LMCT (and a lesser contribution of Vd → Ru^{III} LMCT) because of the significant ruthenium content of β-#131 (Figure 10). The band envelope between ca. 30 000 and 40 000 cm^{-1} contains so many transitions that it is not realistic to make specific assignments. However, it is gratifying that, despite the complexity of the transition envelope, the predicted and experimental peak energies are essentially identical. The predicted spectrum of the restricted spin version of $3H^+$ is also shown in Figure 12 (green trace). It predicts a well-defined shoulder around 14 000 cm^{-1} which is absent from the experimental spectrum. For $3F^+$, weak NIR absorption is again well predicted by DFT. The peak near 8000 cm^{-1} is an acac(−) to Vd(+) LLCT, with some d−d character, while a much weaker shoulder to higher energy is a 4d to Vd(+) MLCT. The strong and relatively pure 4d → π^* Vd(+) transition is #14 calculated at 26 100 cm^{-1}. Multiple transitions then make up the rest of the band envelope to 40 000 cm^{-1} with the strongest being associated with MLCT, LLCT, and internal $\pi-\pi^*$ transitions as assigned. Overall agreement with theory is remarkably good.

The spectrum of $3H^-$ (the only member of the six possible species which could not be isolated) was obtained by the spectroelectrochemical reduction of **3H** in acetonitrile under nitrogen. The species gave well-defined isosbestic points and could be reoxidized spectroelectrochemically to the neutral complex.

The spectra of the anions $3H^-$ and $3F^-$ are shown in Figure 13. In $3H^-$ the NIR band is experimentally observed, albeit it is very weak and assigned to a mix of 4d → Vd(−) MLCT and $\pi-\pi^*$ Vd(−). The intense, allowed 4d → Vd(-) MLCT is observed at rather higher energy as is 4d → acac(−) MLCT (#11,12). Only in this one case is the experimental UV absorption not so well predicted by TD-DFT. For $3F^-$ the LUMO and LUMO+1 are localized primarily on the hfac(−) ligand, and the HOMO is localized on the electron-rich Vd(−) ligand, thus low-lying Vd(−) → hfac(−) LLCT transitions can be expected and are indeed responsible for the predicted weak NIR absorption. Indeed, this species has the most red-shifted transition. However, in this specific case, we were unable to identify any experimental NIR absorption; it may be lost as very weak absorption buried in the visible region tail or may lie below our experimental limit. The anticipated 4d → hfac(−) MLCT transitions are observed at somewhat higher energy.

Overall, there are well-defined trends that can be discerned even though they are partially blurred by the significant mixing. Thus, the 4d → Vd(n) MLCT transitions shift to lower energy from the Vd anion to cation (n, −1 to +1) as would be expected. Uniformly these MLCT transitions in the hfac series lie at higher energy than in the corresponding acac series. Clearly the electron-withdrawing character of the hfac(−) ligand is responsible. The excited state of, for example, the Ru^{II} 4d → Vd(−) MLCT transition is formally Ru^{III} Vd(2−). We have noted above that oxidation or reduction of Vd is accompanied by a shift in charge, from or to the acac(−) ligand, with little change in the net charge on the Ru atom. We could expect the same to be true for these excited states, e.g., that the Ru^{II} 4d → Vd(−) excitation is accompanied by a shift of charge from acac(−) to partially neutralize the change in charge on Ru. This, then, is the mechanism by which these MLCT transitions occur at higher energy in the hfac(−) series.

The Ru 4d → acac(−) MLCT transitions generally increase in energy from Vd anion to cation, though the transition in the **3F** species seems a little lower in energy than expected. These

Table 10. Experimental and TD-DFT Calculated Spectra

index #[a]	exptl (log ε)[b]	energy[c]/10^3 cm^{-1} (oscil. strength f)[c]	assignment[c,d]
			3H$^+$ (HOMO is #130) (in ACN)
1	6.11(2.24)	6.5(0.01)	H-0 → L+0(52%), Ru 4d, acac(−) → Vd(+) MLCT, LLCT
2	11.00sh	10.7(0.001)	H-2 → L+0(76%), Ru 4d → Vd(+) MLCT
3		14.5(0.06)	H-1 → L+0(57%), acac(−) → Vd(+) LLCT
4	17.73(3.75)	17.7(0.15)	H-3 → L+0(46%), acac(−) → Vd(+) LLCT
8	25.4sh	23.2(0.06)	H-5 → L+0(64%), $\pi-\pi^*$ Vd(+), acac(−) → Vd(+) LLCT
12		26.1(0.03)	H-1 → L+1(72%), acac(−) → Vd(+) LLCT
			3H (HOMO is #131α SOMO, 130β) (in DCM)
1	7.17(2.61)	7.6(0.01)	H-0β → L+0(57%), H-1β → L+0(38%), Ru 4d → Vd(0) MLCT, $\pi-\pi^*$ Vd
3	11.31(3.64)	12.3(0.09)	H-1β → L+0(51%), H-0β → L+0(30%), Ru 4d → Vd(0) MLCT, $\pi-\pi^*$ Vd
4	14.45(3.55)	15.0(0.04)	H-0α → L+0(70%), $\pi-\pi^*$ Vd, Ru 4d → Vd(0) MLCT
35	27.3br(3.84)	27.5(0.04)	H-1α → L+3(14%), Ru 4d → Vd(0), acac(−) MLCT
			3H$^-$ (HOMO is #131) (in ACN)
1	11.68(2.89)	12.2(0.02)	H-0 → L+0(96%), Ru 4d → π^* Vd(−) MLCT; $\pi-\pi^*$ Vd(−)
5	18.59(3.81)	17.7(0.03)	H-1 → L+0(80%), Ru 4d → π^* Vd(−) MLCT
6		19.4(0.05)	H-2 → L+0(60%), Ru 4d → π^* Vd(−) MLCT
11	22.42(3.85)	22.5(0.08)	H-2 → L+1(26%), H-1 → L+3(24%), Ru 4d → π^* acac(−), Vd(−) MLCT
12		23.2(0.10)	H-2 → L+2(47%), Ru 4d → π^* acac(−) MLCT
	27.0sh		several weaker transitions
15		24.7(0.03)	H-3 → L+2(33%), H-3 → L+1(23%), H-2 → L+3(20%)
			3F$^+$ (HOMO is #178) (in DCM)
1	7.71(2.51)	8.0(0.004)	H-0 → L+0(69%), acac(−) → Vd(+) LLCT
2	11.0sh	12.4(0.002)	H-2 → L+0(80%), Ru 4d → Vd(+) MLCT
3	17.2(4.04)	16.4(0.17)	H-1 → L+0(54%), acac(−) → Vd(+) LLCT
7	22.60(3.79)	20.8(0.07)	H-4 → L+0(66%), hfac(−) → π^* Vd(+)
11		24.4(0.03)	H-0 → L+1(19%)
13	27.0(3.78_5)	25.5(0.06)	H-0 → L+3(49%)
14		26.1(0.07)	H-2 → L+1(75%), Ru 4d → Vd(+) MLCT
17		27.9(0.03)	H-0 → L+3(26%), H-8 → L+0(26%), H-2 → L+2(22%)
			3F (HOMO is #179α (SOMO), 178β) (in DCM)
1	10.85sh	12.1(0.0002)	H-1α → L+0(21%), H-0β → L+0(21%), Ru 4d → hfac(−), Ru 4d → Vd(0) MLCT
2		12.2(0.003)	H-0β → L+2(28%), H-0α → L+1(28%), Ru 4d → hfac(−) MLCT, Vd(0) → π^* hfac(−) LLCT
3	13.93(3.66)	13.2(0.02)	H-0β → L+0(64%), Ru 4d → Vd(0) MLCT
7	16.81(3.71_5)	15.8(0.05)	H-1β → L+0(76%), Ru 4d → Vd(0) MLCT
18	22.47(3.99)	21.4(0.03)	H-3α → L+0(16%), Ru 4d → hfac(−) MLCT
19		21.7(0.05)	H-3α → L+0(28%), Ru 4d → hfac(−) MLCT
22		22.6(0.05)	H-3β → L+0(64%) $\pi-\pi^*$ Vd(0)
23	23.85sh	23.3(0.04)	H-0β → L+3(44%), Ru 4d → Vd(0) MLCT
	29.4(3.62)		overlap of many weak transitions
			3F$^-$ (HOMO is #179) (in DCM)
1		5.9(0.01)	H-0 → L+0 (90%), Vd(−) → hfac(−) LLCT
2		7.3(0.02)	H-0→ L+1 (92%), Vd(−) → hfac(−) LLCT
3	13.9(3.47)	13.5(0.01)	H-1 → L+0(94%), Ru 4d → hfac(−) MLCT
5		15.1(0.02)	H-0 → L+2 (96%) $\pi-\pi^*$ Vd(−)
8	18.2(3.85)	19.2(0.16)	H-3 → L+0 (52%), H-2 → L+0 (20%), Ru 4d → π^* hfac(−) (MLCT)
11	20.9(3.90_5)	22.4(0.12)	H-3 → L+1 (66%), Ru 4d → π^* hfac(−) (MLCT)
	28.3sh		overlap of many weak transitions

[a] Transition number. [b] Experimental energy/10^3 cm^{-1}, log molar absorbance in parentheses. [c] Derived from TD-DFT calculation; transitions with oscillator strength <0.03 are not shown unless specifically commented upon. [d] Contributions of less than 20% are not shown except when it is comparable to the largest single contribution. In such cases, the excited state is highly mixed with many small contributions. H-1α → L+2 (etc.) signifies transition of an α-electron from HOMO-1 to LUMO+2. ACN = acetonitrile; DCM = dichloromethane.

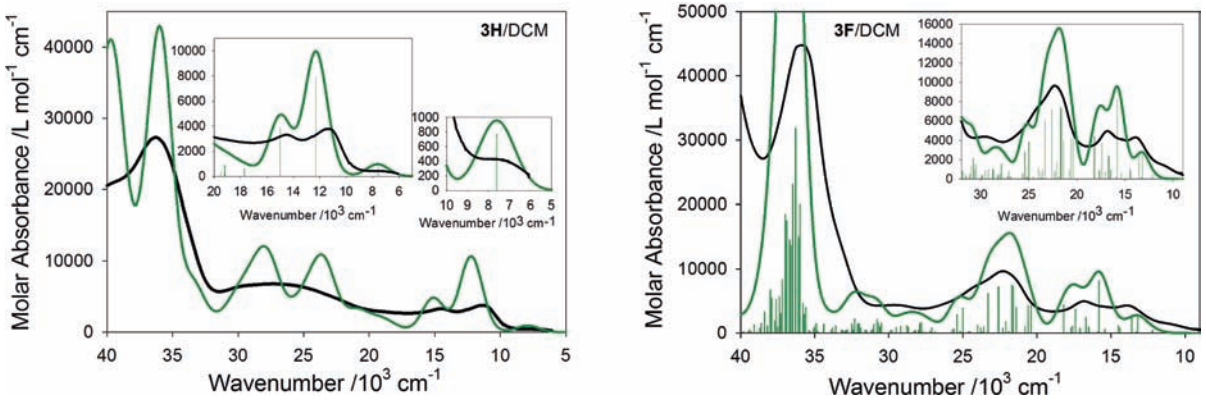

Figure 11. Optical spectra for neutral complexes **3H** (left) and **3F** (right). Experimental data (DCM) (black) and TD-DFT (DCM) calculated spectra (green).

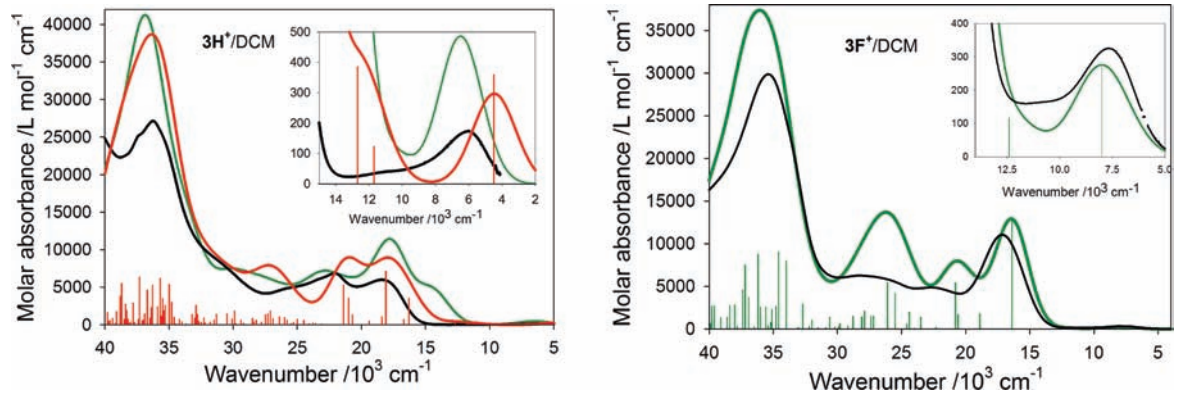

Figure 12. Optical spectra for cationic complexes $\mathbf{3H}^+$ (left) and $\mathbf{3F}^+$ (right). Experimental data (DCM) (black) and TD-DFT ((DCM)) calculated spectra (restricted spin, green; unrestricted spin, **BS**, red).

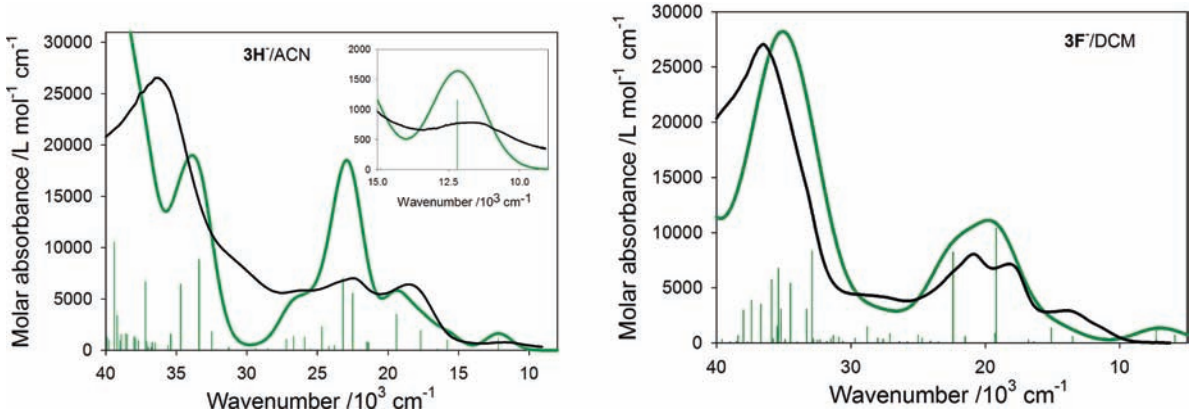

Figure 13. Optical spectra for anionic complexes $\mathbf{3H}^-$ (left) and **3F**− (right). Experimental data (DCM or ACN as noted) (black) and TDDFT calculated spectra (green).

transitions lie, uniformly, at a lower energy in the hfac(−) series, as would be expected. The Vd(n) to acac(−) LLCT transitions increase in energy from Vd anion to cation and lie at lower energy in the hfac(−) series. The reverse transition, acac to Vd(n), obviously lies at the lowest energy with Vd(+), in the NIR, and at the highest energy with Vd(−), again with the higher energy in the hfac(−) group. As an illustration that the actual charge redistribution can be more subtle than discussed above, we display the charge redistribution in the so-called Ru^{II}−Vd(−) MLCT transition (#6) of $\mathbf{3H}^-$ in Figure 14. While this transition has dominantly 4d → Vd(−) character, we note that the charge ends up more on the pyridine fragment of the Vd(−) ligand than the tetrazine. Moreover, there is movement of charge involving the two acac ligands, but one gains charge while the other loses it.

dx.doi.org/10.1021/ja204575u |*J. Am. Chem. Soc.* 2011, 133, 13587–13603

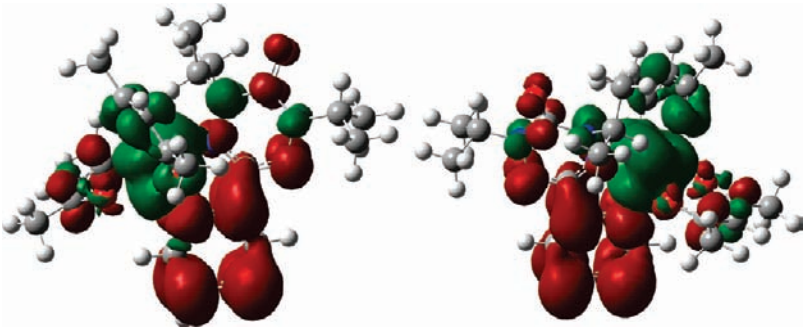

Figure 14. Two views of the charge redistribution in transition #6 of $\mathbf{3H}^{-}$. Charge moves from green to red. The left graphic is oriented to emphasize the 4d → Vd(−) character of the transition. The ketone oxygen lies at the top right. The right graphic is oriented to show that one acac ligand gains charge (lefthand acac) while the other loses charge (top right acac).

SUMMARY

Ruthenium complexes of neutral organic radicals are rare; there are only a handful of phenoxyl radical complexes of ruthenium (most of which are not stable),[62] and the existing ruthenium−nitroxide complexes are based either on Ru_2 tetracarboxylates with axially coordinated nitroxides[63] or mononuclear systems in which the nitroxide radical site is remote from (i.e., not directly coordinated to) ruthenium.[64] The combination of experimental data, combined with the density functional theory results, provides a quite convincing explanation for the optical, electrochemical, and EPR properties of the ruthenium−verdazyl complexes presented here. The availability of the three oxidation states with crystal structures available for five of the six species discussed permits an exceptionally deep comparative probe into the electronic structures of these species. Overall, the neutral and charged ruthenium/verdazyl complexes reveal a new dimension of verdazyl coordination chemistry, namely, their redox active nature as coordinated ligands which hinges on the inherent redox activity of the free verdazyl ligands themselves.[65] To a first (oversimplified) approximation, the anion, neutral, and cation complexes of **3H** and **3F** can be represented as Ru(II) complexes of a verdazyl anion, radical, and cation, respectively. Indeed, oxidation and reduction of the neutral species give ionic complexes in which the unit change in charge on the Vd is partially offset by appreciable redistribution of charge to the acac or hfac ligands; the charge on Ru (Mulliken or NPA) remains relatively constant across series of anion, neutral, and cation. As such, the verdazyl ligand can access a triad of charge states, analogous to the dioxolenes and related redox-active ligands.

However, a closer look at the electronic structure of these complexes reveals a much more subtle interplay of electronic redistribution which does not allow for simple oxidation state identification. The much more strongly electron-donating $Ru(acac)_2$ fragment creates stronger interplay with verdazyl due to Ru(4d) to verdazyl (π^*) backbonding. The magnitude of this interaction is very sensitive to the charge on complex and the nature of the coligands on ruthenium; although ancillary ligand effects on spin distributions in metal−verdazyl complexes have been noted,[25c] the magnitude of the effect in the present systems is without precedent. The strong metal π back-donation creates true metal−ligand noninnocence (as defined by McCleverty and Ward[3] where noninnocent refers to ambiguity of assigning formal charges/oxidation states to ligand/metal). Verdazyl−metal frontier orbital interactions have been investigated in related complexes. Rota et al. have reported calculations on M(II) verdazyl complexes of general structure **4** where M = Ni or Mn. Their analysis accounts for quantitative modeling of metal−radical exchange interactions.[21] However, they could explicitly rule out metal-to-ligand charge transfer and in fact invoke *verdazyl to metal* charge transfer as a significant contributing feature of the magnetism of these complexes. The extent of π donation is not extensive in first row $M(hfac)_2$ systems based on the relatively minimal perturbation of the electronic spectra of these complexes compared to those of the free verdazyl ligand.[18] In sharp contrast, the spectra of all of the $Vd-Ru(LX)_2$ complexes are dominated by charge transfer bands. Clearly, in addition to our observations that the metal coligands play a strong role in the M−Vd interactions, the metal itself dictates how the verdazyl behaves as a coordinated ligand. This suggests that the neutral verdazyl ligand is one which has a significant amount of variability in terms of how it interacts with a coordinated metal ion.

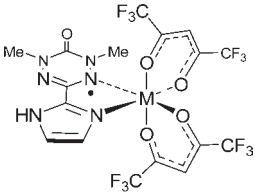

4

EXPERIMENTAL SECTION

General Considerations. All reactions and manipulations were carried out under an argon atmosphere using standard Schlenk or glovebox techniques unless stated otherwise. Solvents were dried and distilled under argon prior to use. All reagents were purchased from Aldrich and used as received. Verdazyl **1a**[26] and $Ru(LX)_2(MeCN)_2$ (LX = acac,[66] hfac[67]) were prepared via literature methods. Verdazyl−Ru complexes **3H** and **3F** were prepared as previously described.[33] Infrared spectra were recorded as KBr pellets using a Perkin-Elmer Spectrum One instrument. UV−vis spectra were recorded using a Cary 50 Scan instrument. EPR spectra were recorded on a Bruker EMX EPR instrument equipped with an X-band microwave bridge. Elemental analyses were carried out by Canadian Microanalytical Services Ltd., Vancouver, BC.

Density functional theory (DFT) calculations employed the Gaussian 03 (revision C.01)[68a] during most of the time this research was being carried out. The Mulliken data, bond orders, and electron populations use this program. We subsequently employed the Gaussian 09 (revision

Table 11. Crystallographic Data

	$3H^+BPh_4^-$	$3F^+BF_4^-$	$CoCp_2^+3F^-$
empirical formula	$C_{99}H_{115}B_2Cl_3N_{10}O_{11}Ru_2$	$C_{23}H_{20}BF_{12}N_5O_5Ru$	$C_{33}H_{30}CoF_{12}N_5O_5Ru$
formula wt.	1951.12	862.32	964.62
T (K)	173	173	103
wavelength (A)	0.71073	0.71073	0.71073
crystal system	monoclinic	triclinic	triclinic
space group	*Cc* (#9)	*P*-1 (#2)	*P*-1 (#2)
a (Å)	10.9465(16)	9.8754(14)	10.6135(3)
b (Å)	28.851(5)	18.263(3)	12.8879(4)
c (Å)	32.054(5)	18.489(3)	14.7751(4)
α (°)	90	96.479(8)	80.475(1)
β (°)	94.241(7)	103.164(5)	87.429(1)
γ (°)	90	90.168(7)	83.043(1)
V (Å^3)	10095 (3)	3224.8(8)	1977.85(10)
Z	4	4	2
μ (cm^{-1})	4.39	6.21	9.03
ρ_{calc} (g/cm^3)	1.284	1.776	1.620
data collected	45391	73747	31708
unique data	11639	14404	9385
parameters	1102	1007	622
g.o.f.	1.00	1.08	1.11
R_1	0.064	0.044	0.033
wR_2	0.095	0.181	0.094
CCDC#	804022	804023	804024

B.01) program[68b] when it became available. The solvation algorithms are slightly different in the two programs which therefore do not provide identical results. The Mulliken charges, bond orders, etc. differ by 1 or 2 in the second decimal place between the two programs. The Gaussian 09 TD-DFT predicted spectra differ in subtle ways from the Gaussian 03 predicted data, but the differences are not significant. Since the differences are so small we did not recalculate the entire problem using Gaussian 09. However, the natural population analysis data appeared more reliable using Gaussian 09. Optimized geometries were calculated using the B3LYP exchange-correlation functional[69] with the LANL2DZ basis set[70] on all elements. Tight SCF convergence criteria (10^{-8} au) were used for all calculations. Vibrational frequency calculations were performed to ensure that the stationary points were minima. Wave functions were checked for stability. Molecular orbital (MO) compositions and the overlap populations between molecular fragments were calculated using the AOMix program[35,71] using the Mulliken scheme.[44,72] Atomic charges were calculated using the Mulliken[44,72] (Gaussian 03) and natural population analysis[48] methods (Gaussian 09 (B.01)) (MPA and NPA, respectively). The analysis of the MO compositions and the charge decomposition analysis was performed using AOMix-CDA.[71] The PCM model[53,73] was used to model solvation assuming dichloromethane as solvent. Time-dependent DFT[56b,73] was used to predict the optical spectra, and the output files were analyzed using the SWIZARD program of Gorelsky.[71] Crystallographic data are given in Table 11.

[1,5-Di-*iso*-propyl-3-(pyridin-2′-yl)-6-oxoverdazyl]bis-(acetylacetonato)ruthenium Tetraphenylborate $3H^+BPh_4^-$. To a solution of **3H** (0.517 g, 0.924 mmol) in a mixture of water (5 mL) and methanol (5 mL) was added $AgNO_3$ (0.157 g, 0.924 mmol). The reaction mixture was stirred for 10 min, during which time the solution turned deep red. The methanol was removed in vacuo and the solution filtered to remove $Ag_{(s)}$. Excess $NaBPh_4$ in water (5 mL) was then added to the solution, and after being left to sit for 10 min, the resulting dark red precipitate was filtered. The crude solid was purified by chromatography (alumina, ACN) followed by recrystallization with $CHCl_3$/ether to give $3H^+BPh_4^-$ as a deep red solid, yield 613 mg (68.0%). Crystals suitable for X-ray crystallography were grown by slow diffusion of ether into a $CHCl_3$ solution. FT-IR (KBr), cm^{-1}: 3052 (w), 2981 (w), 1712 (m), 1550 (s), 1521 (s), 1480 (w), 1366 (m), 1279 (m), 1237 (w), 1125 (w), 1109 (w), 1067 (w), 1030 (w), 939 (w), 744 (w), 733 (w), 705 (m) 607 (w), 459 (w). UV/vis/NIR (DCM), λ_{max}/nm (ε, M^{-1}cm^{-1}): 241(28000), 276(27000), 453(7100), 543(6300), 1645(200). Anal. Calcd for $C_{47}H_{52}N_5O_5BRu\cdot 0.5CHCl_3\cdot 0.5C_4H_{10}O$: C, 60.94; H, 5.94; N, 7.18. Found: C, 60.96; H, 5.74; N, 7.36.

[1,5-Di-*iso*-propyl-3-(pyridin-2′-yl)-6-oxoverdazyl]bis-(hexafluoroacetylacetonato)ruthenium Tetrafluoroborate, $3F^+BF_4^-$. To a solution of **3F** (0.248 g, 0.320 mmol) in DCM (2 mL) was added $AgBF_4$ (0.081 g, 0.320 mmol). The reaction mixture was stirred for 0.5 h, during which time the solution turned from an intense green to an intense blue. The crude mixture was then filtered through a pad of Celite to remove silver metal. After the removal of solvent in vacuo, the crude product was recrystallized from DCM/hexanes to give $3F^+BF_4^-$ as deep blue needles suitable for X-ray crystallography, yield 265 mg (89.9%). FT-IR (KBr), cm^{-1}: 1752 (m), 1597 (m), 1547 (m), 1445 (w), 1431 (w), 1403 (w), 1354 (w), 1299 (m), 1260 (s), 1220 (s), 1155 (s), 1104 (m), 1070 (m), 807 (w), 748 (w), 691 (w), 601 (w). UV/vis/NIR (DCM), λ_{max}/nm (ε, M^{-1}cm^{-1}): 282(30000), 354(6300), 441(4900), 583(11000), 1298(330). Anal. Calcd for $C_{23}H_{20}N_5O_5BF_{16}Ru$: C, 32.04; H, 2.34; N, 8.12. Found: C, 31.84; H, 2.20; N, 8.10.

Cobaltocenium [1,5-Di-*iso*-propyl-3-(pyridin-2′-yl)-6-oxoverdazyl] Bis(hexafluoroacetylacetonato)-ruthenate, $CoCp_2^+3F^-$. To a solution of **3F** (0.102 g, 0.132 mmol) in degassed DCM (5 mL) was added cobaltocene (0.025 g, 0.132 mmol). The reaction mixture was swirled for 10 min, during which time the solution turned from green to red. Degassed hexanes (10 mL) were transferred by canula and layered on the DCM solution. The mixture was allowed to sit undisturbed for several days, during which time large dark crystals formed, yield 100 mg (78.5%). The product is stable in the solid state but quickly oxidizes in solution. FT-IR (KBr), cm^{-1}: 3104 (w), 2973 (w), 1690 (w), 1630 (m), 1582 (w), 1531 (w), 1477 (m), 1418 (w), 1330 (w), 1316 (m), 1261 (s), 1195 (s), 1144 (s), 1136 (s), 1090 (w), 1012 (w), 938 (w), 857 (w), 818 (w), 787 (w), 690 (m), 598 (w), 457 (w). UV/vis (DCM), λ_{max}/nm (ε, M^{-1}cm^{-1}): 479(8000), 549(7100), 715(2900). Anal. Calcd for $C_{33}H_{30}F_{12}N_5O_5RuCo$: C, 41.09; H, 3.13; N, 7.26. Found: C, 41.37; H, 2.67; N, 6.85.

■ ASSOCIATED CONTENT

Supporting Information. Complete refs 68a,68b, crystallographic details (as CIF files), and computational details (structural data and TD-DFT predicted electronic spectra). This material is available free of charge via the Internet at http://pubs.acs.org.

■ AUTHOR INFORMATION

Corresponding Author
rhicks@uvic.ca

■ ACKNOWLEDGMENT

We thank the Natural Sciences and Engineering Research Council of Canada for support. We also thank Dr. Leo Slep, Departamento de Química Inorgánica, Analítica y Química Física, Universidad de Buenos Aires, for help with the COT analysis. Computational work was made possible by the facilities

of the Shared Hierarchical Academic Research Computing Network, Ontario, Canada (http://www.sharcnet.ca).

REFERENCES

(1) (a) Jorgensen, C. K. *Coord. Chem. Rev.* **1966**, *1*, 164.(b) Jorgensen, C. K., *Oxidation Numbers and Oxidation States*; Springer-Verlag: New York, 1969.

(2) Chaudhuri, P.; Verani, C. N.; Bill, E.; Bothe, E.; Weyhermuller, T.; Wieghardt, K. *J. Am. Chem. Soc.* **2001**, *123*, 2213.

(3) Ward, M. D.; McCleverty, J. A. *J. Chem. Soc., Dalton Trans.* **2002**, 275.

(4) (a) Kaim, W.; Schwederski, B.; Heilmann, O.; Hornung, F. M. *Coord. Chem. Rev.* **1999**, *182*, 323. (b) Kaim, W. *Dalton Trans.* **2003**, 761. (c) Kaim, W.; Schwederski, B. *Pure Appl. Chem.* **2004**, *76*, 351. (d) Kaim, W.; Schwederski, B. *Coord. Chem. Rev.* **2010**, *254*, 1580.

(5) Chirik, P. J.; Wieghardt, K. *Science* **2010**, *327*, 794.

(6) (a) Wada, T.; Tsuge, K.; Tanaka, K. *Chem. Lett.* **2000**, 910. (b) Wada, T.; Tsuge, K.; Tanaka, K. *Angew. Chem., Int. Ed.* **2000**, *39*, 1479. (c) Wada, T.; Tsuge, K.; Tanaka, K. *Inorg. Chem.* **2001**, *40*, 329. (d) Bouwkamp, M. W.; Bowman, A. C.; Lobkovsky, E.; Chirik, P. J. *J. Am. Chem. Soc.* **2006**, *128*, 13340. (e) Haneline, M. R.; Heyduk, A. F. *J. Am. Chem. Soc.* **2006**, *128*, 8410. (f) Miyazato, Y.; Wada, T.; Tanaka, K. *Bull. Chem. Soc. Jpn.* **2006**, *79*, 745. (g) Polyansky, D.; Cabelli, D.; Muckerman, J. T.; Fujita, E.; Koizumi, T.; Fukushima, T.; Wada, T.; Tanaka, K. *Angew. Chem., Int. Ed.* **2007**, *46*, 4169. (h) Stanciu, C.; Jones, M. E.; Fanwick, P. E.; Abu-Omar, M. M. *J. Am. Chem. Soc.* **2007**, *129*, 12400. (i) Blackmore, K. J.; Lal, N.; Ziller, J. W.; Heyduk, A. F. *J. Am. Chem. Soc.* **2008**, *130*, 2728. (j) Muckerman, J. T.; Polyansky, D. E.; Wada, T.; Tanaka, K.; Fujita, E. *Inorg. Chem.* **2008**, *47*, 1787. (k) Ringenberg, M. R.; Kokatam, S. L.; Heiden, Z. M.; Rauchfuss, T. B. *J. Am. Chem. Soc.* **2008**, *130*, 788. (l) Rolle, C. J.; Hardcastle, K. I.; Soper, J. D. *Inorg. Chem.* **2008**, *47*, 1892. (m) Zarkesh, R. A.; Ziller, J. W.; Heyduk, A. F. *Angew. Chem., Int. Ed.* **2008**, *47*, 4715. (n) Nguyen, A. I.; Blackmore, K. J.; Carter, S. M.; Zarkesh, R. A.; Heyduk, A. F. *J. Am. Chem. Soc.* **2009**, *131*, 3307. (o) Boyer, J. L.; Rochford, J.; Tsai, M. K.; Muckerman, J. T.; Fujita, E. *Coord. Chem. Rev.* **2010**, *254*, 309. (p) Lippert, C. A.; Arnstein, S. A.; Sherrill, C. D.; Soper, J. D. *J. Am. Chem. Soc.* **2010**, *132*, 3879. (q) Lippert, C. A.; Soper, J. D. *Inorg. Chem.* **2010**, *49*, 3682. (r) Smith, A. L.; Clapp, L. A.; Hardcastle, K. I.; Soper, J. D. *Polyhedron* **2010**, *29*, 164.

(7) (a) McCleverty, J. A. *Prog. Inorg. Chem.* **1968**, *10*, 49. (b) Robertson, N.; Cronin, L. *Coord. Chem. Rev.* **2002**, *227*, 93.

(8) (a) Pierpont, C. G.; Buchanan, R. M. *Coord. Chem. Rev.* **1981**, *38*, 45. (b) Pierpont, C. G.; Lange, C. W. *Prog. Inorg. Chem.* **1994**, *41*, 331.

(9) (a) Gorelsky, S. I.; Dodsworth, E. S.; Lever, A. B. P.; Vlcek, A. A. *Coord. Chem. Rev.* **1998**, *174*, 469. (b) Ittel, S. D.; Johnson, L. K.; Brookhart, M. *Chem. Rev.* **2000**, *100*, 1169. (c) Lever, A. B. P.; Gorelsky, S. I. *Coord. Chem. Rev.* **2000**, *208*, 153. (d) Hill, N. J.; Vargas-Baca, I.; Cowley, A. H. *Dalton Trans.* **2009**, 240. (e) Lever, A. B. P. *Coord. Chem. Rev.* **2010**, *254*, 1397.

(10) Lu, C. C.; Bill, E.; Weyhermuller, T.; Bothe, E.; Wieghardt, K. *J. Am. Chem. Soc.* **2008**, *130*, 3181.

(11) Knijnenburg, Q.; Gambarotta, S.; Budzelaar, P. H. M. *Dalton Trans.* **2006**, 5442.

(12) (a) Thomas, F. *Eur. J. Inorg. Chem.* **2007**, 2379.(b) Thomas, F. In *Stable Radicals: Fundamentals and Applied Aspects of Odd-Electron Compounds*; Hicks, R. G., Ed.; Wiley: Wiltshire, 2010; p 281.

(13) Whittaker, J. W. *Chem. Rev.* **2003**, *103*, 2347.

(14) Sheldon, R. A.; Arends, I. *J. Mol. Catal. A* **2006**, *251*, 200.

(15) (a) Donati, N.; Konigsmann, M.; Stein, D.; Udino, L.; Grutzmacher, H. *C. R. Chim.* **2007**, *10*, 721. (b) Konigsmann, M.; Donati, N.; Stein, D.; Schonberg, H.; Harmer, J.; Sreekanth, A.; Grutzmacher, H. *Angew. Chem., Int. Ed.* **2007**, *46*, 3567.

(16) Hicks, R. G. In *Stable Radicals: Fundamentals and Applied Aspects of Odd-Electron Compounds*; Hicks, R. G., Ed.; Wiley: Wiltshire, 2010; p 245.

(17) Brook, D. J. R.; Lynch, V.; Conklin, B.; Fox, M. A. *J. Am. Chem. Soc.* **1997**, *119*, 5155.

(18) Hicks, R. G.; Lemaire, M. T.; Thompson, L. K.; Barclay, T. M. *J. Am. Chem. Soc.* **2000**, *122*, 8077.

(19) (a) Barclay, T. M.; Hicks, R. G.; Lemaire, M. T.; Thompson, L. K. *Inorg. Chem.* **2001**, *40*, 5581. (b) Norel, L.; Pointillart, F.; Train, C.; Chamoreau, L. M.; Boubekeur, K.; Journaux, Y.; Brieger, A.; Brook, D. J. R. *Inorg. Chem.* **2008**, *47*, 2396.

(20) Barclay, T. M.; Hicks, R. G.; Lemaire, M. T.; Thompson, L. K. *Inorg. Chem.* **2003**, *42*, 2261.

(21) Rota, J. B.; Norel, L.; Train, C.; Ben Amor, N.; Maynau, D.; Robert, V. *J. Am. Chem. Soc.* **2008**, *130*, 10380.

(22) Barclay, T. M.; Hicks, R. G.; Lemaire, M. T.; Thompson, L. K.; Xu, Z. Q. *Chem. Commun.* **2002**, 1688.

(23) Lemaire, M. T.; Barclay, T. M.; Thompson, L. K.; Hicks, R. G. *Inorg. Chim. Acta* **2006**, *359*, 2616.

(24) Barclay, T. M.; Hicks, R. G.; Lemaire, M. T.; Thompson, L. K. *Chem. Commun.* **2000**, 2141.

(25) (a) Brook, D. J. R.; Fornell, S.; Noll, B.; Yee, G. T.; Koch, T. H. *J. Chem. Soc., Dalton Trans.* **2000**, 2019. (b) Barclay, T. M.; Hicks, R. G.; Lemaire, M. T.; Thompson, L. K. *Inorg. Chem.* **2001**, *40*, 6521. (c) Brook, D. J. R.; Abeyta, V. *J. Chem. Soc., Dalton Trans.* **2002**, 4219. (d) Stevens, J. E.; Brook, D. J. R.; Abeyta, V. W. *Polyhedron* **2003**, *22*, 2241.

(26) Gilroy, J. B.; Koivisto, B. D.; McDonald, R.; Ferguson, M. J.; Hicks, R. G. *J. Mater. Chem.* **2006**, *16*, 2618.

(27) (a) Rota, J. B.; Calzado, C. J.; Train, C.; Robert, V. *J. Chem. Phys.* **2010**, *132*, #154742. (b) Yakovenko, A. V.; Kolotilov, S. V.; Cador, O.; Golhen, S.; Ouahab, L.; Pavlishchuk, V. V. *Eur. J. Inorg. Chem.* **2009**, 2354.

(28) Brook, D. J. R.; Fornell, S.; Stevens, J. E.; Noll, B.; Koch, T. H.; Eisfeld, W. *Inorg. Chem.* **2000**, *39*, 562.

(29) Wu, J. Z.; Bouwman, E.; Reedijk, J.; Mills, A. M.; Spek, A. L. *Inorg. Chim. Acta* **2003**, *351*, 326.

(30) (a) Nakabayashi, K.; Ozaki, Y.; Kawano, M.; Fujita, M. *Angew. Chem., Int. Ed.* **2008**, *47*, 2046. (b) Ozaki, Y.; Kawano, M.; Fujita, M. *Chem. Commun.* **2009**, 4245.

(31) Pointillart, F.; Train, C.; Herson, P.; Marrot, J.; Verdaguer, M. *New J. Chem.* **2007**, *31*, 1001.

(32) Norel, L.; Chamoreau, L. M.; Journaux, Y.; Oms, O.; Chastanet, G.; Train, C. *Chem. Commun.* **2009**, 2381.

(33) McKinnon, S. D. J.; Patrick, B. O.; Lever, A. B. P.; Hicks, R. G. *Chem. Commun.* **2010**, *46*, 773.

(34) (a) Gorelsky, S. I.; Lever, A. B. P. *Int. J. Quantum Chem.* **2000**, *80*, 636. (b) Gorelsky, S. I.; Lever, A. B. P.; Ebadi, M. *Coord. Chem. Rev.* **2002**, *230*, 97.

(35) Gorelsky, S. I.; Lever, A. B. P. *J. Organomet. Chem.* **2001**, *635*, 187.

(36) (a) Li, J.; Xu, L. C.; Chen, J. C.; Zheng, K. C.; Ji, L. N. *J. Phys. Chem. A* **2006**, *110*, 8174. (b) Remenyi, C.; Kaupp, M. *J. Am. Chem. Soc.* **2005**, *127*, 11399.

(37) (a) Al-Noaimi, M.; El-Khateeb, M.; Haddad, S. F.; Sunjuk, M.; Crutchley, R. J. *Polyhedron* **2008**, *27*, 3239. (b) Ess, D. H.; Nielsen, R. J.; Goddard, W. A.; Periana, R. A. *J. Am. Chem. Soc.* **2009**, *131*, 11686.

(38) Futera, Z.; Klenko, J.; Sponer, J. E.; Sponer, J.; Burda, J. V. *J. Comput. Chem.* **2009**, *30*, 1758.

(39) (a) Spikes, G. H.; Sproules, S.; Bill, E.; Weyhermuller, T.; Wieghardt, K. *Inorg. Chem.* **2008**, *47*, 10935. (b) Dovletoglou, A.; Adeyemi, S. A.; Meyer., T. J. *Inorg. Chem.* **1996**, *35*, 4120. (c) Taube, H. *Pure Appl. Chem.* **1979**, *51*, 901.

(40) Frenking, G.; Frohlich, N. *Chem. Rev.* **2000**, *100*, 717.

(41) Gorelsky, S. I.; Solomon, E. I. *Theor. Chem. Acc.* **2008**, *119*, 57.

(42) (a) Kotyk, M. W.; Gorelsky, S. I.; Conrad, J. C.; Carra, C.; Fogg, D. E. *Organometallics* **2009**, *28*, 5424. (b) Solomon, E. I.; Gorelsky, S. I.; Dey, A. *J. Comput. Chem.* **2006**, *27*, 1415.

(43) Gilroy, J. B.; McKinnon, S. D. J.; Kennepohl, P.; Zsombor, M. S.; Ferguson, M. J.; Thompson, L. K.; Hicks, R. G. *J. Org. Chem.* **2007**, *72*, 8062.

(44) Mulliken, R. S. *J. Chem. Phys.* **1955**, *23*, 1841.

(45) Stout, E. W.; Politzer, P. *Theor. Chim. Acta* **1968**, *12*, 379.

(46) Mayer, I. *Chem. Phys. Lett.* **1983**, *97*, 270.

(47) Pauling, L. *The Nature of the Chemical Bond*; Cornell University Press: Ithaca, 1960.
(48) Reed, A. E.; Curtiss, L. A.; Weinhold, F. *Chem. Rev.* **1988**, *88*, 899.
(49) Herebian, D.; Wieghardt, K. E.; Neese, F. *J. Am. Chem. Soc.* **2003**, *125*, 10997.
(50) Ruiz, E.; Alemany, P.; Alvarez, S.; Cano, J. *J. Am. Chem. Soc.* **1997**, *119*, 1297.
(51) Grapperhaus, C. A.; Bill, E.; Weyhermuller, T.; Neese, F.; Wieghardt, K. *Inorg. Chem.* **2001**, *40*, 4191.
(52) Bachler, V.; Olbrich, G.; Neese, F.; Wieghardt, K. *Inorg. Chem.* **2002**, *41*, 4179.
(53) Noodleman, L.; Lovell, T.; Han, W. G.; Torres, R. A.; Himo, F. *Comprehensive Coordination Chemistry II*; Elsevier: Oxford, 2004; p 491.
(54) (a) Caballol, R.; Castell, O.; Illas, F.; Moreira, P. R.; Malrieu, J. P. *J. Phys. Chem. A* **1997**, *101*, 7860. (b) Hopmann, K. H.; Conradie, J.; Ghosh, A. *J. Phys. Chem. B* **2009**, *113*, 10540. (c) Lovell, T.; Han, W. G.; Liu, T. Q.; Noodleman, L. *J. Am. Chem. Soc.* **2002**, *124*, 5890. (d) Nair, N. N.; Schreiner, E.; Pollet, R.; Staemmler, V.; Marx, D. *J. Chem. Theory Comput.* **2008**, *4*, 1174. (e) Prushan, M. J.; Tomezsko, D. M.; Lofland, S.; Zeller, M.; Hunter, A. D. *Inorg. Chim. Acta* **2007**, *360*, 2245.
(55) (a) Bachler, V.; Chaudhuri, P.; Wieghardt, K. *Chem.—Eur. J.* **2001**, *7*, 404. (b) Ghosh, M.; Weyhermuller, T.; Wieghardt, K. *Dalton Trans.* **2008**, 5149. (c) Grapperhaus, C. A.; Kozlowski, P. M.; Kumar, D.; Frye, H. N.; Venna, K. B.; Poturovic, S. *Angew. Chem., Int. Ed.* **2007**, *46*, 4085. (d) Guihery, N.; Robert, V.; Neese, F. *J. Phys. Chem. A* **2008**, *112*, 12975. (e) Herebian, D.; Bothe, E.; Neese, F.; Weyhermuller, T.; Wieghardt, K. *J. Am. Chem. Soc.* **2003**, *125*, 9116. (f) Kapre, R. R.; Bothe, E.; Weyhermuller, T.; George, S. D.; Muresan, N.; Wieghard, K. *Inorg. Chem.* **2007**, *46*, 7827. (g) Kokatam, S.; Ray, K.; Pap, J.; Bill, E.; Geiger, W. E.; LeSuer, R. J.; Rieger, P. H.; Weyhermuller, T.; Neese, F.; Wieghardt, K. *Inorg. Chem.* **2007**, *46*, 1100. (h) Samanta, S.; Singh, P.; Fiedler, J.; Zalis, S.; Kaim, W.; Goswami, S. *Inorg. Chem.* **2008**, *47*, 1625. (i) Sanyal, A.; Chatterjee, S.; Castineiras, A.; Sarkar, B.; Singh, P.; Fiedler, J.; Zalis, S.; Kaim, W.; Goswami, S. *Inorg. Chem.* **2007**, *46*, 8584.
(56) (a) Blanchard, S.; Neese, F.; Bothe, E.; Bill, E.; Weyhermuller, T.; Wieghardt, K. *Inorg. Chem.* **2005**, *44*, 3636. (b) Neese, F. *Coord. Chem. Rev.* **2009**, *253*, 526.
(57) (a) Amos, A. T.; Hall, G. G. *Proc. R. Soc. London A* **1961**, *263*, 483. (b) King, H. F.; Stanton, R. E.; Kim, H.; Wyatt, R. E.; Parr, R. G. *J. Chem. Phys.* **1967**, *47*, 1936.
(58) (a) Bart, S. C.; Chlopek, K.; Bill, E.; Bouwkamp, M. W.; Lobkovsky, E.; Neese, F.; Wieghardt, K.; Chirik, P. J. *J. Am. Chem. Soc.* **2006**, *128*, 13901. (b) Soda, T.; Kitagawa, Y.; Onishi, T.; Takano, Y.; Shigeta, Y.; Nagao, H.; Yoshioka, Y.; Yamaguchi, K. *Chem. Phys. Lett.* **2000**, *319*, 223. (c) Yamaguchi, K.; Jensen, F.; Dorigo, A.; Houk, K. N. *Chem. Phys. Lett.* **1988**, *149*, 537.
(59) Neese, F. *J. Phys. Chem. Solids* **2004**, *65*, 781.
(60) (a) Chlopek, K.; Bothe, E.; Neese, F.; Weyhermuller, T.; Wieghardt, K. *Inorg. Chem.* **2006**, *45*, 6298. (b) Ghosh, P.; Bill, E.; Weyhermuller, T.; Neese, F.; Wieghardt, K. *J. Am. Chem. Soc.* **2003**, *125*, 1293.
(61) (a) Magnuson, R. H.; Taube, H. *J. Am. Chem. Soc.* **1975**, *97*, 5129.(b) Lever, A. B. P. *Inorganic Electronic Spectroscopy*; Elsevier: Amsterdam, 1984.
(62) (a) Patra, S.; Sarkar, B.; Maji, S.; Fiedler, J.; Urbanos, F. A.; Jimenez-Aparicio, R.; Kaim, W.; Lahiri, G. K. *Chem.—Eur. J.* **2006**, *12*, 489. (b) Mishra, H.; Mukherjee, R. *J. Organomet. Chem.* **2007**, *692*, 3248. (c) Roy, N.; Sproules, S.; Weyhermuller, T.; Wieghardt, K. *Inorg. Chem.* **2009**, *48*, 3783.
(63) (a) Handa, M.; Sayama, Y.; Mikuriya, M.; Nukada, R.; Hiromitsu, I.; Kasuga, K. *Bull. Chem. Soc. Jpn.* **1995**, *68*, 1647. (b) Handa, M.; Sayama, Y.; Mikuriya, M.; Nukada, R.; Hiromitsu, I.; Kasuga, K. *Chem. Lett.* **1996**, 201. (c) Handa, M.; Sayama, Y.; Mikuriya, M.; Nukada, R.; Hiromitsu, I.; Kasuga, K. *Bull. Chem. Soc. Jpn.* **1998**, *71*, 119. (d) Sayama, Y.; Handa, M.; Mikuriya, M.; Hiromitsu, I.; Kasuga, K. *Chem. Lett.* **1998**, 777. (e) Sayama, Y.; Handa, M.; Mikuriya, M.; Hiromitsu, I.; Kasuga, K. *Chem. Lett.* **1999**, 453. (f) Sayama, Y.; Handa, M.; Mikuriya, M.; Hiromitsu, I.; Kasuga, K. *Bull. Chem. Soc. Jpn.* **2000**, *73*, 2499. (g) Sayama, Y.; Handa, M.; Mikuriya, M.; Hiromitsu, I.; Kasuga, K. *Bull. Chem. Soc. Jpn.* **2001**, *74*, 2129. (h) Sayama, Y.; Handa, M.; Mikuriya, M.; Hiromitsu, I.; Kasuga, K. *Bull. Chem. Soc. Jpn.* **2003**, *76*, 769.
(64) (a) Ottaviani, M. F.; Ghatlia, N. D.; Bossmann, S. H.; Barton, J. K.; Durr, H.; Turro, N. J. *J. Am. Chem. Soc.* **1992**, *114*, 8946. (b) Ottaviani, M. F.; Ghatlia, N. D.; Turro, N. J. *J. Phys. Chem.* **1992**, *96*, 6075. (c) Ottaviani, M. F.; Turro, C.; Turro, N. J.; Bossmann, S. H.; Tomalia, D. A. *J. Phys. Chem.* **1996**, *100*, 13667. (d) Hintermaier, F.; Beck, W. *Polyhedron* **1998**, *17*, 483. (e) Leznoff, D. B.; Rancurel, C.; Sutter, J. P.; Rettig, S. J.; Pink, M.; Kahn, O. *Organometallics* **1999**, *18*, 5097. (f) Pointillart, F.; Bernot, K.; Colas, J.; Sorace, L.; Sessoli, R. *Inorg. Chim. Acta* **2008**, *361*, 3427.
(65) Gilroy, J. B.; McKinnon, S. D. J.; Koivisto, B. D.; Hicks, R. G. *Org. Lett.* **2007**, *9*, 4837.
(66) Kobayashi, T.; Nishina, Y.; Shimizu, K.; Sato, G. P. *Chem. Lett.* **1988**, 1137.
(67) Baird, I. R.; Rettig, S. J.; James, B. R.; Skov, K. A. *Can. J. Chem.* **1999**, *77*, 1821.
(68) (a) Frisch, M. J. et al. *Gaussian 03* (revision C.0), Gaussian, Inc.: Wallingford, CT, 2004. (b) Frisch, M. J. et al. *Gaussian 09* (revision B.01), Gaussian, Inc.: Wallingford, CT, 2009.
(69) Lee, C. T.; Yang, W. T.; Parr, R. G. *Phys. Rev. B* **1988**, *37*, 785.
(70) (a) Dunning, T. H.; Hay, P. J. *Modern Theoretical Chemistry*; Plenum: New York, 1976; Vol. 3, p 1. (b) Hay, P. J.; Wadt, W. R. *J. Chem. Phys.* **1985**, *82*, 270. (c) Hay, P. J.; Wadt, W. R. *J. Chem. Phys.* **1985**, *82*, 299.
(71) Gorelsky, S. I. *AOMIX-CDA and SWIZARD Programs*, http://www.sg-chem.net/, 2005.
(72) (a) Mulliken, R. S. *J. Chem. Phys.* **1955**, *23*, 2338. (b) Mulliken, R. S. *J. Chem. Phys.* **1955**, *23*, 2343. (c) Mulliken, R. S. *J. Chem. Phys.* **1955**, *23*, 1833.
(73) Bickelhaupt, F. M.; Baerends, E. J. *Reviews in Computational Chemistry*; Wiley: New York, 2000; Vol. 15, p 1.